1521-0111/103/2/100–112$35.00
MOLECULAR PHARMACOLOGY

dx.doi.org/10.1124/molpharm.122.000555
Mol Pharmacol 103:100–112, February 2023

A Complete Endocannabinoid Signaling System Modulates Synaptic Transmission between Human Induced Pluripotent Stem Cell–Derived Neurons

Melissa J. Asher, Hannah M. McMullan, Ao Dong, Yulong Li, and Stanley A. Thayer

Department of Pharmacology (M.J.A., H.M.M., S.A.T.), Graduate Program in Neuroscience (M.J.A., S.A.T.), and Molecular Pharmacology and Therapeutics Graduate Program (H.M.M., S.A.T.), University of Minnesota Medical School, Minneapolis, Minnesota; State Key Laboratory of Membrane Biology, Peking University School of Life Sciences (A.D., Y.L.), IDG/McGovern Institute for Brain Research (A.D., Y.L.), and Peking-Tsinghua Center for Life Sciences, Academy for Advanced Interdisciplinary Studies (A.D., Y.L.), Peking University, Beijing, China; and Chinese Institute for Brain Research, Beijing, China (Y.L.)

Received May 6, 2022; accepted October 24, 2022

ABSTRACT

The endocannabinoid system (ECS) modulates synaptic function to regulate many aspects of neurophysiology. It adapts to environmental changes and is affected by disease. Thus, the ECS presents an important target for therapeutic development. Despite recent interest in cannabinoid-based treatments, few preclinical studies are conducted in human systems. Human induced pluripotent stem cells (hiPSCs) provide one possible solution to this issue. However, it is not known if these cells have a fully functional ECS. Here, we show that hiPSC-derived neuron/astrocyte cultures exhibit a complete ECS. Using Ca^{2+} imaging and a genetically encoded endocannabinoid sensor, we demonstrate that they not only respond to exogenously applied cannabinoids but also produce and metabolize endocannabinoids. Synaptically driven $[Ca^{2+}]_i$ spiking activity was inhibited (EC_{50} = 48 ± 13 nM) by the efficacious agonist [R(+)-[2,3-dihydro-5-methyl-3-[(morpholinyl)methyl]pyrolol [1,2,3-de]-1,4-benzoxazin-yl]-(1-naphthalenyl)methanone mesylate] (Win 55,212-2) and by the endogenous ligand 2-arachidonoyl glycerol (2-AG; EC_{50} = 2.0 ± 0.6 μm). The effects of Win 55212-2 were blocked by a CB_1 receptor-selective antagonist. Δ^9-Tetrahydrocannabinol acted as a partial agonist, maximally inhibiting synaptic activity by 47 ± 14% (EC_{50} = 1.4 ± 1.9 μm). Carbachol stimulated 2-AG production in a manner that was independent of Ca^{2+} and blocked by selective inhibition of diacylglycerol lipase. 2-AG returned to basal levels via a process mediated by monoacylglycerol lipase as indicated by slowed recovery in cultures treated with 4-[*Bis*(1,3-benzodioxol-5-yl)hydroxymethyl]-1-piperidinecarboxylic acid 4-nitrophenyl ester (JZL 184). Win 55,212-2 markedly desensitized CB_1 receptor function following a 1-day exposure, whereas desensitization was incomplete following 7-day treatment with JZL 184. This human cell culture model is well suited for functional analysis of the ECS and as a platform for drug development.

SIGNIFICANCE STATEMENT

Despite known differences between the human response to cannabinoids and that of other species, an in vitro human model demonstrating a fully functional endocannabinoid system has not been described. Human induced pluripotent stem cells (hiPSCs) can be obtained from skin samples and then reprogrammed into neurons for use in basic research and drug screening. Here, we show that hiPSC-derived neuronal cultures exhibit a complete endocannabinoid system suitable for mechanistic studies and drug discovery.

Introduction

The endocannabinoid (eCB) system (ECS) regulates processes ranging from appetite and emesis to mood and memory (Lowe et al., 2021; Lu and Mackie, 2021). As our understanding of the ECS in health and disease continues to develop,

This work was made possible by National Institutes of Health grants from the National Institute on Drug Abuse [Grant DA07304] (to S.A.T.) and the National Institute of Mental Health [Grant MH122193] (to S.A.T.) and support from the Viral Vector and Cloning Core/Viral Innovation Core [Grant P30 DA048742-01A1].

No author has an actual or perceived conflict of interest with the contents of this article.

dx.doi.org/10.1124/molpharm.122.000555.

ABBREVIATIONS: $[Ca^{2+}]_i$, intracellular Ca^{2+} concentration; $[Mg^{2+}]_o$, extracellular Mg^{2+} concentration; ΔF/Fo, change in fluorescence intensity relative to the resting fluorescence intensity; Δ^9-THC, Δ^9-tetrahydrocannabinol; 2-AG, 2-arachidonoyl glycerol; AAV, adeno-associated virus; AMPA, α-amino-3-hydroxy-5-methyl-4-isoxazolepropionic acid; AUC, area under the curve; BDNF, brain-derived neurotrophic factor; $CB_{1/2}$R, cannabinoid type 1 and 2 receptor; CNQX, 6-cyano-7-nitroquinoxaline-2,3-dione; DAG, diacylglycerol; DMEM/F-12, Dulbecco's Modified Eagle Medium/Ham's F12 Medium; DO34, (3-(Phenylmethyl)-4-[[4-[4-(trifluoromethoxy)phenyl]-1H-1,2,3-triazol-1-yl]carbonyl]-1-piperazinecarboxylic acid,1, 1-dimethylethyl ester,(2-Benzyl-4-{[(2-methyl-2-propanyl)oxy]carbonyl}piperazinyl){4-[(4-trifluoromethoxy)phenyl]-1H-1,2,3-triazol-1-yl}methanone); eCB, endocannabinoid; ECS, eCB system; ER, endoplasmic reticulum; GDNF, glial cell–derived neurotrophic factor; HHSS, HEPES-buffered Hanks' salt solution; hiPSC, human induced pluripotent stem cell; JZL 184, 4-[Bis(1,3-benzodioxol-5-yl)hydroxymethyl]-1-piperidinecarboxylic acid 4-nitrophenyl ester; MAG, monoacylglycerol; MSE, metabotropic suppression of excitation; NESS 0327, N-piperidinyl-[8-chloro-1-(2,4-dichlorophenyl)-14,5,6-tetrahydrobenzo [6,7]cyclohepta[1,2-c]pyrazole-3-carboxamide]; NMDA, N-methyl-D-aspartate; ROI, region of interest; Win-2, [R(+)-[2,3-dihydro-5-methyl-3-[(morpholinyl)methyl]pyrolol [1,2,3-de]-1,4-benzoxazin-yl]-(1-naphthalenyl)methanone mesylate] (WIN 55,212-2).

there is increasing interest in this system as a therapeutic target (Di Marzo, 2018; Wilkerson et al., 2021). The ECS presents several sites for drug action. It is composed of cannabinoid type 1 and 2 receptors ($CB_{1/2}$Rs), eCB ligands, and lipases that produce eCBs on demand from membrane lipids or hydrolyze them to terminate signaling.

CB_1Rs are primarily expressed in neurons and are widely distributed throughout the central nervous system (Glass et al., 1997). The principal active ingredient in cannabis, Δ^9-tetrahydrocannabinol (Δ^9-THC), exerts its psychoactive effects via CB_1R (Matsuda et al., 1990). CB_1R agonists are approved for use as antiemetics and appetite stimulants (Garcia and Shamliyan, 2018) and show potential for treating seizures (Rosenberg et al., 2017), pain (Fowler, 2021), and anxiety (deRoon-Cassini et al., 2020). On-target adverse effects have generated considerable interest in developing agonists biased toward desired therapeutic signaling pathways (Leo and Abood, 2021). Much of the preclinical work on CB_1R ligands is performed on rodent neurons because human brain tissue is relatively unavailable. However, rodent models have limitations. For example, ECS neurodevelopment differs between rodents and humans, influencing the effects of cannabinoids on synaptic plasticity (Bara et al., 2021), and human neurons are more sensitive than rodent neurons to seizure-causing drugs (Tukker et al., 2020). It is of particular importance to pharmacological studies that human and rodent CB_1Rs differ in their distribution and their affinities to a range of ligands (McPartland et al., 2007).

In vitro models with a complete ECS are useful for understanding how ECS components are affected by $CB_{1/2}$R ligands as well as how the ECS adapts to disease conditions. For example, the ECS is affected by and modulates stress in the human brain (deRoon-Cassini et al., 2020). Furthermore, when the ECS as a whole is considered as a therapeutic target, modulating eCB metabolism emerges as an important strategy that preserves the spatial and temporal aspects of endogenous signaling. Indeed, clinical trials for inhibitors of metabolic enzymes, which are thought to be less likely than receptor agonists to produce tolerance or psychoactive side effects, are ongoing (van Egmond et al., 2021). Although exciting progress has been made, obstacles to clinical drug development remain. In vitro models suitable for long-term study are lacking, and human models with a fully functional ECS have not been described.

Human induced pluripotent stem cells (hiPSCs) are one potential solution to this problem. hiPSCs are derived from somatic cells, such as skin fibroblasts, which can be obtained much more easily and less invasively than brain tissue. Exogenous expression of factors necessary for pluripotency reprograms fibroblasts into pluripotent stem cells, capable of differentiating into all three embryonic germ layers (Takahashi et al., 2007). These iPSCs are then differentiated into cultures resembling target cell type(s). iPSC-derived neurons offer a minimally invasive in vitro human model for basic research and drug development, with the potential for long-term and high-throughput studies.

hiPSC-derived neuronal cultures therefore show promise as a tool for studying the ECS. Previous studies have shown that CB_1R is expressed in hiPSCs and hiPSC-derived neurons (Bobrov et al., 2017) and that Δ^9-THC can affect development (Stanslowsky et al., 2017) and gene expression (Guennewig et al., 2018) in these cells. In cortical spheroids derived from hiPSCs, the components of the ECS are expressed, and CB_1Rs appear functional because rimonabant, an inverse agonist of CB_1Rs, altered the development of excitatory synapses (Papariello et al., 2021). However, to our knowledge, there have been no functional studies of cannabinoid agonists on neural activity in hiPSC-derived neurons, and whether the components of an ECS beyond CB_1Rs are functional is not known.

In this study, we demonstrate the presence of a fully functional ECS in a commercially available line of hiPSC-derived neuron/astrocyte cultures. In this model system, CBs modulate synaptic activity, and 2-arachidonoyl glycerol (2-AG) is synthesized by diacylglycerol (DAG) lipase upon stimulation and metabolized via monoacylglycerol (MAG) lipase. We characterize the Ca^{2+} sensitivity of 2-AG synthesis, demonstrating the utility of these cultures for mechanistic studies. We also compare a receptor agonist to a MAG lipase inhibitor for their ability to desensitize CB_1R-mediated inhibition of synaptic activity, showing the feasibility of long-term (7-day) treatment protocols with these cultures. This human cell culture model is well suited for functional analysis of the ECS and for screening drugs for actions on its components.

Materials and Methods

Reagents. Penicillin/streptomycin (catalog number: 15140) was from Thermo Fisher Scientific (Carlsbad, CA); BrainPhys Neuronal Medium with SM1 (catalog number: 05792), human recombinant brain-derived neurotrophic factor (catalog number: 78005), and human recombinant glial cell-derived neurotrophic factor (catalog number: 78058) were from Stem Cell Technologies (Vancouver, BC, Canada); NeuralX medium with cortical supplement (catalog number: 500005-250) was from StemoniX (Maple Grove, MN); HEPES (catalog number: H4034), calcium chloride (catalog number: C3881),(3-(Phenylmethyl)-4-[[4-[4-(trifluoromethoxy)phenyl]-1H-1,2,3-triazol-1-yl]carbonyl]-1-piperazinecarboxylic acid,1, 1-dimethylethyl ester,(2-Benzyl-4-{[(2-methyl-2-propanyl)oxy]carbonyl}piperazinyl){4-[(4-trifluoromethoxy)phenyl]-1H-1,2,3-triazol-1-yl}methanone) (DO34; catalog number: SML2732) and Win 55,212-2 (Win-2; catalog number: 131543-23-2) were from Millipore Sigma (St. Louis, MO); 2-AG (catalog number: 62610), N-piperidinyl-[8-chloro-1-(2,4-dichlorophenyl)-1,4,5,6-tetrahydrobenzo [6,7]cyclohepta[1,2-c]pyrazole-3-carboxamide] (NESS 0327; catalog number: 10004184), 4-[Bis(1,3-benzodioxol-5-yl)hydroxymethyl]-1-piperidinecarboxylic acid 4-nitrophenyl ester (JZL 184; catalog number: 13158), and Win 55,212-2 (catalog number: 10009023) were from Cayman Chemical (Ann Arbor, MI); 6-cyano-7-nitroquinoxaline-2,3-dione (CNQX; catalog number: 1045), dihydroxyphenylglycine (catalog number: 0805), carbachol (catalog number: 2810), and MK 801 (catalog number: 0924) were from Tocris Biosciences (Minneapolis, MN); FLIPR Calcium 6 dye (catalog number: R8190) was from Molecular Devices (San Jose, CA); and Δ^9-THC was from the National Institute on Drug Abuse Drug Supply Program (Research Triangle Institute, Research Triangle Park, NC). Dulbecco's Modified Eagle Medium/Ham's F12 Medium (DMEM/F-12; catalog number: 11330-032), Neurobasal Medium (catalog number: 21103-049), B27 Supplement (catalog number: 17504-044), N2 Supplement (catalog number: 17502-048), and GlutaMax (catalog number: 35050-061) were from Life Technologies (Carlsbad, CA). Matrigel (catalog number: 356273) was from Corning (Glendale, AZ). For experiments using cells obtained from BrainXell, brain-derived neurotrophic factor (BDNF; catalog number: 450-02), glial cell-derived neurotrophic factor (GDNF; catalog number: 450-10), and transforming growth factor β1 (catalog number: 100-21C) were from PeproTech (East Windsor, NJ).

Human iPSC–Derived Neuronal Cultures. Human iPSC–derived neuron/astrocyte cultures in 96-well plates (catalog number: BCARX-AA-0096) were obtained from StemoniX, Inc. (Maple Grove, MN) and were received 8–10 weeks after plating. Upon receipt, transfer medium was replaced with BrainPhys medium supplemented with 1% SM1 and human recombinant brain-derived neurotrophic factor and human recombinant glial cell-derived neurotrophic factor (both at 20 ng/mL) via one 75% media change followed by one 50% media change. Culture medium was exchanged 50% with fresh BrainPhys medium every 2 to 3 days. Cultures were maintained in a humidified atmosphere of 5% CO_2/95% air (pH 7.4) at 37°C. To allow for recovery from shipping, cells were maintained for a minimum of 7 days before starting experiments. These mixed neuronal-astrocyte cultures contain 90% glutamatergic and 10% GABAergic neurons (StemoniX, Inc. Technical Summary: Cellular Identity in microbrain assay ready cultures).

In a subset of experiments, hiPSC-derived neurons were obtained from BrainXell (Madison, WI) and Applied StemCell, Inc. (Milpitas, CA) (BX-0300 and ASE-9741-C, respectively). Cultures were produced according to manufacturers' instructions. Briefly, BrainXell hiPSCs were suspended in seeding media comprised of a 1:1 mixture of DMEM/F-12:Neurobasal supplemented with B27, N2, seeding supplement, supplement K, 0.5 mM GlutaMax, 15 μg/mL Matrigel, 10 ng/mL BDNF, 10 ng/mL GDNF, and 10 ng/mL transforming growth factor β1 and plated (45,000 cells per well) in a 96-well plate (Greiner; catalog number 655892) precoated with poly-D-lysine. Four days after plating, cells were fed with media without Matrigel and in which the seeding supplement was replaced with day-4 supplement. After the day-4 feeding, cells were fed every 3 days with media comprised of a 1:1 mixture of DMEM/F-12:Neurobasal supplemented with B27, N2, supplement K, 0.5 mM GlutaMax, 10 ng/mL BDNF, and 10 ng/mL GDNF. Experiments were performed 14–17 days after plating. Applied StemCell, Inc. hiPSCs (30,000 cells per well) were suspended in proprietary cortical neuron culture media (ASE-9741MM), spun at 250 x *g*, resuspended in cortical neuron culture media, and plated on a Matrigel-coated 96-well plate. Cultures were fed every 2 days, and experiments were performed 14 to 15 days after plating.

Viral Vectors. PHP.eB adeno-associated virus (AAV) vectors were produced by the Viral Vector and Cloning Core facility at the University of Minnesota following standard packaging procedures (Chen et al., 2019). The pRC-PHP.eB packaging plasmid was a gift from Dr. Viviana Gradinaru (California Institute of Technology; Chan et al., 2017).

The $GRAB_{eCB2.0}$ plasmid was described previously (Dong et al., 2022); $AAV_{PHP.eB}$-hSYN-$GRAB_{eCB2.0}$ virus was used at a titer of 3.68×10^{11} genome copies per mL. The hSyn-eGFP plasmid was a gift from Dr. Bryan Roth (Addgene plasmid #50465); $AAV_{PHP.eB}$-hSYN-GFP virus was used at a titer of 1.30×10^{11} genome copies per mL. The GFAP-mCherry plasmid was produced by the University of Minnesota Viral Vector Core from pAAV-GFAP-hM4D(Gi)-mCherry, which was a gift from Bryan Roth (Addgene plasmid #50479). $AAV_{PHP.eB}$-GFAP-mCherry virus was used at a titer of 1.41×10^{11} genome copies per mL. Viruses were added to cultures at the indicated titers immediately after a routine media change 6–12 days before imaging.

Image Acquisition. All images were acquired on a Nikon A1 laser scanning confocal system with a Nikon ECLIPSE Ti inverted microscope (Nikon, Melville, NY) using Nikon Elements software (version 5.02.01). An infrared z-positioning device (Nikon Perfect Focus System) was used to prevent drift in the z-dimension during acquisition of time courses. Cultures were maintained at 37°C and 5% CO_2 in a stage-top incubator (Chamlide) modified to hold 96-well plates. Breathe-Easy gas-permeable plate sealing membranes (Research Products International, Mt. Prospect, IL) were used to prevent contamination of wells that were not actively being imaged.

hSYN-eGFP and GFAP-mCherry Expression. Cultures expressing hSYN-eGFP and GFAP-mCherry were imaged 6 days after infection. Culture medium was replaced with HEPES-buffered Hanks' concentration($[Mg^{2+}]_o$) before imaging to reduce background fluorescence. Twelve-bit 1024 × 1024–pixel images were acquired using a Nikon Plan Apochromat λ 60× oil objective (numerical aperture = 1.4, refractive index = 1.515). eGFP was excited at 488 nm, with emission detected at 550 nm (50 nm band pass); mCherry was excited at 561 nm, with emission detected at 600 nm (50 nm band pass). The pinhole was set to 1 Airy unit with one-directional imaging. Channels were captured sequentially using a GaAsP detector, and no averaging was performed. Each image was captured as a 20-μm z-stack (voxel size = 0.2072 × 0.2072 × 1 μm^3). The example image in Fig. 1 is represented as a maximum intensity z-projection.

Calcium Imaging. To visualize calcium events in the hiPSC-derived cultures, 25% of the media in the well was replaced with prewarmed FLIPR Calcium 6 dye (Molecular Devices) dissolved in HHSS. Cells were incubated in dye at 37°C and 5% CO_2 for 1.5–2 hours before imaging. Two minutes before imaging, the culture medium was fully exchanged twice with HHSS containing either 0.9 mM (normal) or 0.1 mM (low) Mg^{2+}.

Twelve-bit 512 × 512–pixel images (pixel size = 1.1525 × 1.1525 μm^2) were acquired with a Nikon Plan Apochromat VC 20× DIC N2 20× air objective (numerical aperture = 0.75). The Calcium 6 dye was excited at 488 nm, with emission detected at 550 nm (50 nm band pass), and the pinhole was set to 1 Airy unit with one-directional imaging. Images were recorded using a GaAsP detector, and no averaging was performed.

Calcium imaging data were analyzed with a custom ImageJ macro. Briefly, background was subtracted using the rolling ball method (radius 250 μm), and frames were registered using ImageJ's "Correct 3D Drift" function. A maximum intensity projection of the registered image was thresholded and segmented into regions of interest (ROIs) using ImageJ's "Analyze particles" function. Average intensity for each ROI in each frame of the image was calculated and converted to the change in fluorescence intensity relative to the resting fluorescence intensity ($\Delta F/F_o$) values, using the minimum value for each ROI as F_o. Traces were manually quality checked, and ROIs were eliminated if they 1) were not fully in the field of view for the entire recording, 2) did not show activity in 0.1 mM Mg^{2+} (raw intensity amplitude of at least 50 to distinguish from noise) during experiments in which changes in this activity were of interest rather than the presence or absence of activity, i.e., those other than Figs. 1 and 8), or 3) had an unstable baseline, defined as a change of more than 20% within the baseline epoch before addition of drug. Wells with fewer than 10 ROIs after quality checking were excluded from further analysis. The area under the curve (AUC) was calculated by summing the $\Delta F/F_0$ values in each imaging epoch. The response to drugs and treatments is expressed as a percent change in AUC before and after adding drug.

GRAB eCB Imaging. Cultures expressing $GRAB_{eCB2.0}$ were imaged 6–12 days after infection. The $GRAB_{eCB.2.0}$ sensor was excited at 488 nm, with emission detected at 550 nm (50 nm band pass). The pinhole was set to 1 Airy unit with one-directional imaging. Images were recorded using a GaAsP detector, and no averaging was performed. Before imaging, the media was replaced with HHSS (0.9 mM $[Mg^{2+}]_o$) to reduce background fluorescence. To better capture multiple fine processes in focus, each frame was acquired as a 3-slice z-stack, with slices 1 μm apart (voxel size 0.2072 × 0.2072 × 1 μm^3), and ROIs were chosen and analyzed using maximum intensity z-projections.

For initial proof of concept and time course of $GRAB_{eCB2.0}$ activation (Fig. 5), 12-bit 1024 × 1024–pixel images were acquired using a Nikon Plan Apochromat 60× oil objective (numerical aperture = 1.4, refractive index = 1.515). Each frame consisted of one 3-slice z-stack (voxel size = 0.2072 × 0.2072 × 1 μm^3), and frames were automatically acquired every 20 seconds during each epoch as follows: baseline, starting 2 minutes after a media change to HHSS and continuing for 1 minute (4 frames); carbachol, starting 10 seconds after the addition of 1 μm carbachol and continuing for 3 minutes (10

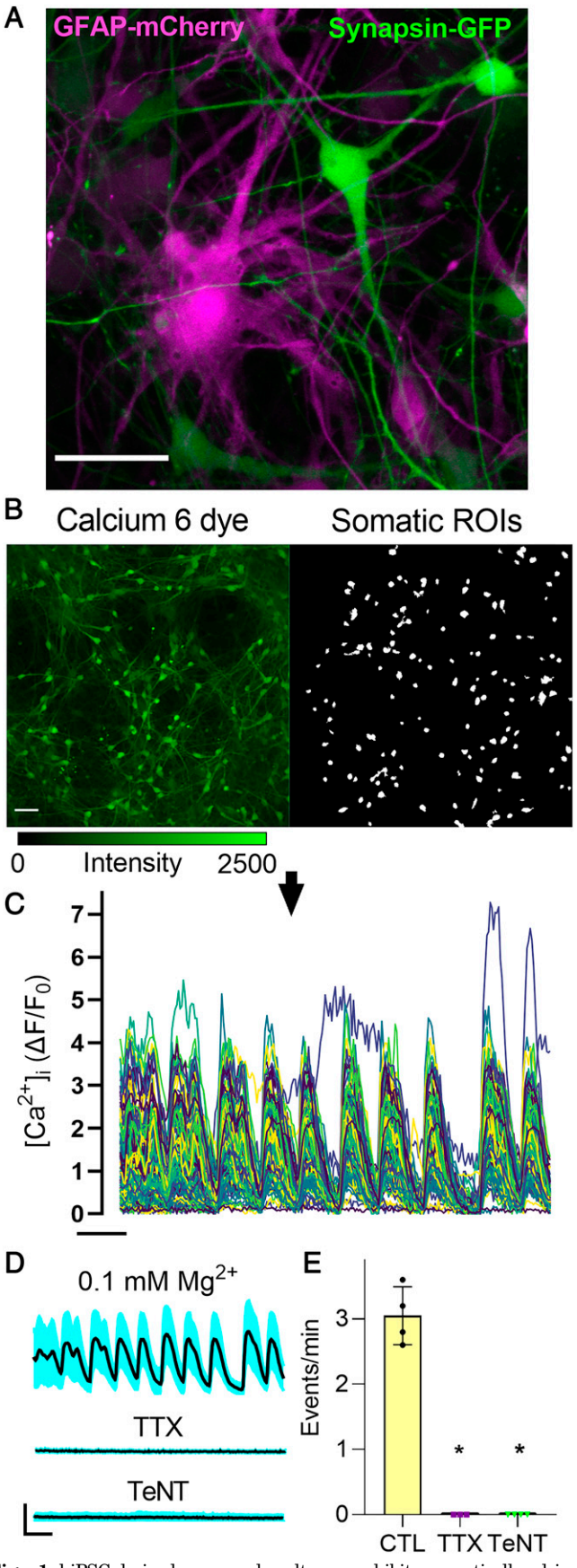

Fig. 1. hiPSC-derived neuronal cultures exhibit synaptically driven $[Ca^{2+}]_i$ spiking. (A) hiPSC-derived neuronal cultures expressing mCherry from the GFAP promoter (magenta) and GFP from the synapsin promoter (green). Scale bar, 50 μm. (B) Representative image of hiPSC-derived cultures in Calcium 6 dye (left) and ROIs derived from this image using threshold-based segmentation in ImageJ (right). Scale bar, 50 μm. (C) Individual $[Ca^{2+}]_i$ traces representing $\Delta F/F_0$ for each ROI in (B). Scale bar, 30 seconds. (D) Representative traces show mean $[Ca^{2+}]_i$ (solid line) from a single field of hiPSC-derived neuronal cells (S.D. denoted by blue shading) in 0.1 mM Mg^{2+} buffer containing H_2O vehicle (top), 10 μm tetrodotoxin (TTX, middle), or pretreated (18 hours) with 2.5 μm tetanus toxin (TeNT, bottom). Scale bars: horizontal, 30 seconds; vertical, 1.0 $\Delta F/F_0$. Bar graph summarizes Ca^{2+} spiking activity (events per minute) in cultures treated with H_2O vehicle (CTL), TTX, or TeNT as depicted in traces. *$P < 0.05$ relative to CTL. Kruskal-Wallis test with Dunn's multiple comparisons correction, $P = 0.024$ for TTX and 0.013 for TeNT relative to vehicle, $n = 3$ to 4 wells per treatment.

frames); and Win-2, starting 10 seconds after the addition of 300 nM Win-2 and continuing for 3 minutes (10 frames). The total time elapsed between each epoch was 30 seconds.

To quickly image a larger field of view containing processes from multiple cells (Figs. 6–8), lower-magnification and lower-resolution 12-bit 512 × 512–pixel images (voxel size = 1.1525 × 1.1525 × 1 μm^3) were acquired with a Nikon Plan Apochromat VC 20× DIC N2 20× air objective (numerical aperture = 0.75). In preliminary studies, carbachol-induced GRAB fluorescence consistently peaked by 50 seconds after addition of carbachol, and Win-2–induced GRAB fluorescence reached a steady state after 2 to 3 minutes. Therefore, five frames were acquired 10 seconds apart for each epoch, with baseline starting 2 minutes after a complete media change to HHSS buffer to reduce background fluorescence, carbachol starting 10 seconds after addition of carbachol, and Win-2 starting 2.5 minutes after addition of Win-2. Cells were incubated with drug or vehicle in media/Calcium 6 dye mixture for 1 hour (DO34 and JZL 184)] or 30 minutes (thapsigargin) before imaging, and the drug concentration was maintained in HHSS throughout image acquisition.

Images were analyzed using ImageJ. Briefly, frames were registered using ImageJ's "Correct 3D drift" plugin, and regions of interest were drawn manually with the polygon tool around processes that expressed the GRAB sensor (i.e., showed robust fluorescence in the presence of Win-2). Only the Win-2 epoch was considered when selecting ROIs; the investigator was blinded to treatment condition and to the appearance of the processes during the carbachol epoch. Average intensity in each frame was calculated for four ROIs plus one ellipsoid background region per image, with the four ROIs selected from different quadrants of the image wherever possible. Background-corrected average intensities were used to calculate $\Delta F/F_o$ for each ROI in each frame, with the baseline epoch average used as F_o. Because brightness varied considerably between individual processes, data are reported as a percentage of the Win-2 epoch average. The average peak $\Delta F/F_o$ (normalized to Win-2) of all ROIs in a well was considered as $n = 1$.

Desensitization. To test for receptor desensitization, cells were pretreated with 0.1% DMSO, 1 μM Win-2, or 1 μM JZL 184 (added with a half media change containing 2× drug during regular feeding) for 15 minutes (acute treatment) or 1, 3, or 7 days (chronic treatments). For 7-day treatments, drugs were included in fresh media at 1× during scheduled feedings; 1- and 3-day treatments were not long enough to require feeding. Immediately before imaging, the pretreated drugs were washed out using four 5-minute washes in 0.9 mM Mg^{2+} HHSS containing 0.5% fatty acid-free bovine serum albumin (75% media change with each wash). After washing, cells were placed in 0.1 mM Mg^{2+} HHSS and imaged before and after the addition of Win-2 as described in *Calcium Imaging* above.

Experimental Design and Statistical Analysis. Controls and experimental groups were run in parallel to minimize effects of time or individual experiments. For all experiments, an individual sample ($n = 1$) is defined as the average of all ROIs in a single well, and each experiment was replicated on two to three independent platings of cells. For desensitization experiments, sample size was predetermined

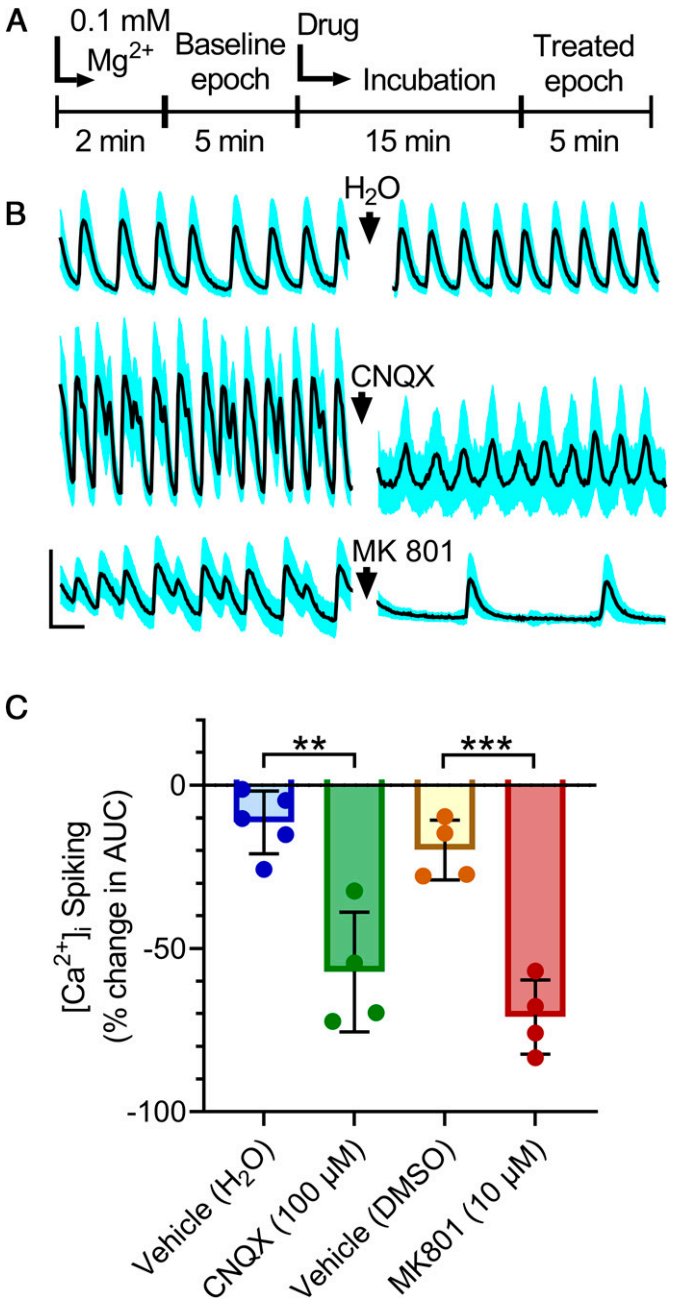

Fig. 2. hiPSC-derived neuronal cultures form a glutamatergic synaptic network. (A) Schematic shows drug treatments sequence for this and following figures. (B) Representative traces show mean $[Ca^{2+}]_i$ (solid line) for a single field of hiPSC-derived neuronal cells (S.D. denoted by blue shading) in 0.1 mM Mg^{2+} buffer before (baseline epoch) and after (treated epoch) the addition of vehicle (H_2O, top), 100 µM CNQX (middle), or 10 µM MK801 (bottom). Scale bars: horizontal, 30 seconds; vertical, 1.0 $\Delta F/F_0$. (C) Bar graph summarizes the change in $[Ca^{2+}]_i$ spiking activity (percentage of change in AUC) before and after adding vehicle (H_2O for CNQX and DMSO for MK 801), 100 µM CNQX, or 10 µM MK 801. $^{**}P < 0.01$ relative to vehicle control; $^{***}P < 0.001$ relative to vehicle. Data are presented as mean ± S.D. Student's t test: t = 4.9 and $P = 0.002$ for CNQX relative to H_2O; t = 7.0 and $P = 0.0004$ for MK 801 relative to DMSO; $n = 4$ to 5 wells per condition.

using GPower software (version 3.1) for an effect size of 0.5 and a power of 0.8; other sample sizes were not predetermined but conform to similar studies. For ROI selection in $GRAB_{eCB2.0}$ imaging experiments, the investigator was blinded to treatment condition and to the culture's response during the experimental carbachol epoch; calcium imaging experiments relied on automated algorithms and objective exclusion criteria (described in *Calcium Imaging* above) without blinding. Cultures used in Figs. 1–9 were derived from a single adult male donor.

Statistical analyses and hypothesis testing were performed using GraphPad Prism (version 9.2.0), aside from concentration-response curve fitting, which was performed using OriginPro 2019 (version 9.6.0). Data are presented as mean ± S.D. The Shapiro-Wilk test was used to test for normality, and Levene's test was used to test for homogeneity of variance. Nonparametric data were analyzed with the Mann-Whitney U test. For normally distributed data with homogeneous variance, Student's t test (unpaired, two-tailed) was used for two-group comparisons, one- or two-way ANOVA with Tukey's post hoc test for comparisons of multiple groups, and two-way repeated measures ANOVA with Tukey's post hoc test for time courses. The Brown-Forsythe ANOVA with Dunnet's T3 multiple comparisons test was used for comparisons of multiple groups with nonhomogeneous variance. Statistical significance was defined as $P < 0.05$. No tests for outliers were performed.

Results

hiPSC-Derived Neurons Form a Glutamatergic Signaling Network in Vitro. hiPSC-derived neuronal cultures consisted of a mix of neuron-like cells and astrocyte-like cells, as evidenced by morphology and the fact that they expressed fluorescent markers from the neuron-selective human synapsin (hSyn-GFP) and astrocyte-selective glial fibrillary acidic protein (GFAP-mCherry) promoters, respectively (Fig. 1A). The neuronal cells extended fine processes that, in a previous study, were shown to express synaptic markers (Green et al., 2019). In this study, we examined these cultures for the elements of a functional eCB system.

To study synaptic transmission between hiPSC-derived neurons, we evoked synaptically driven intracellular Ca^{2+} concentration ($[Ca^{2+}]_i$) spiking activity. Previous studies of synaptic networks in primary cultures of rat neurons have shown that reducing the extracellular Mg^{2+} concentration ($[Mg^{2+}]_o$) will evoke paroxysmal epileptiform bursts of action potentials that produce $[Ca^{2+}]_i$ spikes that are driven by glutamatergic synaptic activity (McLeod et al., 1998). Bathing the culture in buffer containing 0.1 mM Mg^{2+} evoked repetitive $[Ca^{2+}]_i$ spikes detected by confocal imaging of cultures loaded with FLIPR Calcium 6 dye (Molecular Devices). Ca^{2+} levels in the cell body of neuronal cells were measured from somatic ROIs defined by applying a threshold-based segmentation to the fluorescence image as described in *Methods*. The individual ROI traces shown in Fig. 1C showed that the $[Ca^{2+}]_i$ oscillated in a seizure-like synchronized pattern. In 0.1 mM $[Mg^{2+}]_o$, the $[Ca^{2+}]_i$ spiking frequency was 3 ± 0.4 events per minute (Fig. 1D). This activity was blocked completely by 10 µm tetrodotoxin, which blocks action potentials, and by 18-hour preincubation with 2.5 µm tetanus toxin, which prevents neurotransmitter release. Thus, the 0.1 mM $[Mg^{2+}]_o$-evoked repetitive $[Ca^{2+}]_i$ spiking, although recorded from the soma, represents synaptic activity between networked hiPSC-derived neurons.

To study the pharmacology of this network activity, the following treatment protocol was employed (Fig. 2A). Cell culture media was replaced with HEPES-buffered Hank's salt solution containing 0.1 mM $[Mg^{2+}]_o$, and the cultures were allowed to stabilize for 2 minutes. A 5-minute baseline epoch was recorded, which served as control for the experiment. Then, 50% of the well volume was exchanged with

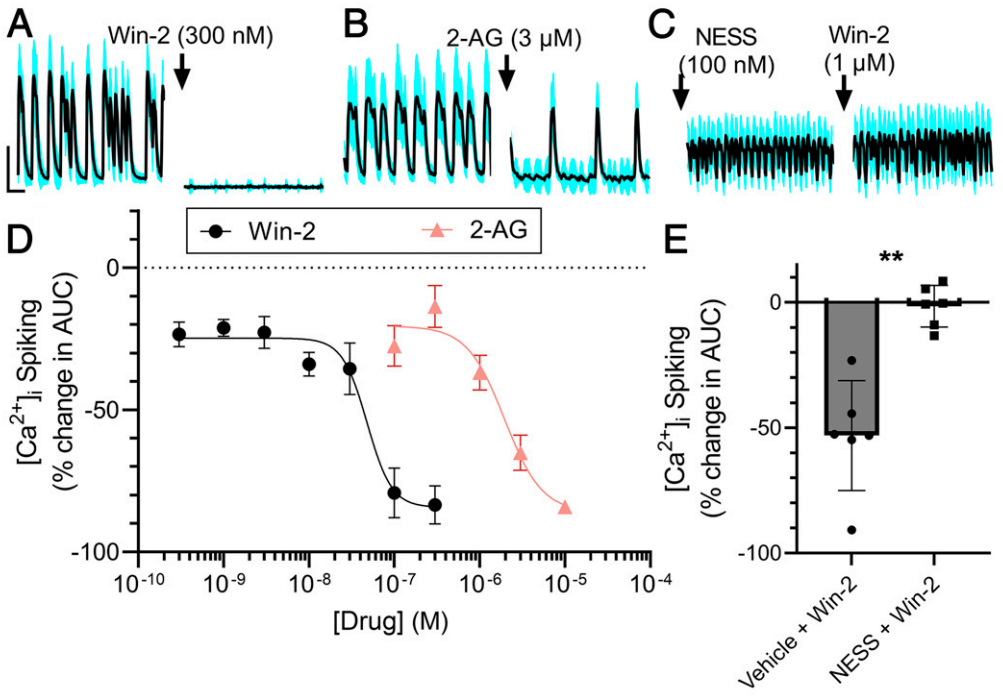

Fig. 3. Cannabinoid agonists inhibit synaptic activity between hiPSC- derived neurons via CB_1R. (A–C) Representative traces show mean (solid) $[Ca^{2+}]_i$ ($\Delta F/F_0$) of a single field of hiPSC-derived neuronal cells (S.D. denoted by blue shading) in 0.1 mM Mg^{2+} buffer before and after the addition of 300 nM Win-2 (A), 3 μM 2-AG (B), or 1 μM Win-2 in the presence of 100 nM NESS 0327 (C). Scale bars: horizontal, 30 seconds; vertical, 1.0 $\Delta F/F^0$. (D) Concentration-response curves for Win-2 (circles) and 2-AG (triangles) were fit with a logistic equation of the form: percentage of change in AUC = $A_1 + [(A_2\text{-}A_1)/(1 + 10^{((\log x\text{-}x)p)})]$, where $x_0 = EC_{50}$, x = log[drug], A_1 = percentage of change in the absence of drug, A_2 = percentage of change at a maximally effective drug concentration, and p = slope factor. The following values were calculated using a nonlinear, least-squares curve-fitting program: $A_1 = -25\%$ for Win-2 and -21% for 2-AG; $A_2 = -84\%$ for Win-2 and -86% for 2-AG; $EC_{50} = 48 \pm 13$ nM for Win-2 and 2.0 ± 0.6 μM for 2-AG; $p = -3.0 \pm 1.4$ for Win-2 and -2.0 ± 1.0 for 2-AG. $n = 4$–6 wells per concentration. (E) Bar graph summarizes change in $[Ca^{2+}]_i$ spiking induced by 1 μM Win-2 in wells treated with vehicle (0.1% ethanol, left) or 100 nM NESS 0327 (right). Data are presented as mean ± S.D. $^{**}P < 0.01$. Welch's t test, $t_{(6.4)} = 5.4$, $P = 0.0014$, 6 wells per condition.

0.1 mM $[Mg^{2+}]_o$ containing drug or vehicle at twice the final concentration and was incubated for 15 minutes. Finally, a 5-minute treated epoch was recorded. $[Ca^{2+}]_i$ spiking activity was quantified by measuring the AUC for the average $\Delta F/F_o$ of the FLIPR Calcium 6 dye for all active ROIs in the imaging field. Drug effects were quantified by determining the change in AUC during the treated epoch relative to the initial baseline epoch (percentage of change in AUC).

Synchronous $[Ca^{2+}]_i$ spiking activity was stable in vehicle-treated wells (Fig. 2, B and C). The N-methyl-D-aspartate (NMDA) receptor antagonist MK 801 (10 μm) inhibited $[Ca^{2+}]_i$ spiking by 71 ± 11%, whereas the α-amino-3-hydroxy-5-methyl-4-isoxazolepropionic acid (AMPA) receptor antagonist CNQX (100 μM) inhibited the synaptic activity by 57 ± 18%. Thus, glutamatergic synaptic transmission drives a large portion of the $[Ca^{2+}]_i$ spiking activity. CNQX significantly inhibited both frequency ($U = 4$; $P < 0.05$) and amplitude ($t_{(9)} = 3.7$; $P < 0.01$) of the $[Ca^{2+}]_i$ spiking. [(+)-5-Methyl-10,11-dihydroxy-5H-dibenzo(a,d)cyclohepten-5,10-imine] (MK801) significantly inhibited $[Ca^{2+}]_i$ spiking frequency ($t_{(6)} = 4.3$; $P < 0.01$) but did not significantly affect $[Ca^{2+}]_i$ spike amplitude ($t_{(6)} = 1.9$; $P = 0.1$). Thus, we used AUC as a measure of $[Ca^{2+}]_i$ spiking activity to capture both effects. The contributions of NMDA and AMPA receptors are consistent with research showing that the low $[Mg^{2+}]_o$ model of epileptiform activity depends on NMDA receptor activation with a smaller contribution from AMPA receptors (Gulyás-Kovács et al., 2002). These results show that hiPSC-derived neuronal cultures contain cells that resemble neurons morphologically and functionally and that form a glutamatergic signaling network in vitro that could potentially be manipulated by cannabinoids.

hiPSC-Derived Neurons Are Sensitive to Exogenous Cannabinoids. We next tested whether the low $[Mg^{2+}]_o$-induced synaptic activity between hiPSC-derived neurons was sensitive to cannabinoid receptor agonists. The potent synthetic agonist Win-2 produced a concentration-dependent decrease in both the amplitude and frequency of $[Ca^{2+}]_i$ spikes (Fig. 3, A and D). The IC_{50} for Win-2–mediated inhibition of $[Ca^{2+}]_i$ spiking was 48 ± 13 nM, an 18-fold lower potency relative to that described for inhibition of synaptic activity in rodent models (Shen et al., 1996). The inhibition of $[Ca^{2+}]_i$ spiking by Win-2 was completely blocked by the selective CB_1 R antagonist NESS 0327 (Ruiu et al., 2003) (Fig. 3, C and E), indicating that Win-2 acted on functional CB_1Rs in these neurons. Application of 100 nM NESS 0327 did not consistently increase $[Ca^{2+}]_i$ spiking activity ($t_{(14)} = 1.9$ $P = 0.07$), suggesting that eCB tone was not sufficiently elevated under these conditions to suppress synaptic transmission.

An endogenous ligand for CB_1Rs, 2-AG, also inhibited 0.1 mM $[Mg^{2+}]_o$-evoked $[Ca^{2+}]_i$ spiking (Fig. 2, B and D). The IC_{50} for 2-AG–mediated inhibition of $[Ca^{2+}]_i$ spiking was 2.0 ± 0.6 μM. The lower potency relative to Win-2 is consistent with that previously described in rodent models (Straiker and Mackie, 2005). The potency of 2-AG for inhibiton of glutamatergic synaptic activity in hiPSC cultures is fivefold lower than that described for inhibition of synaptic

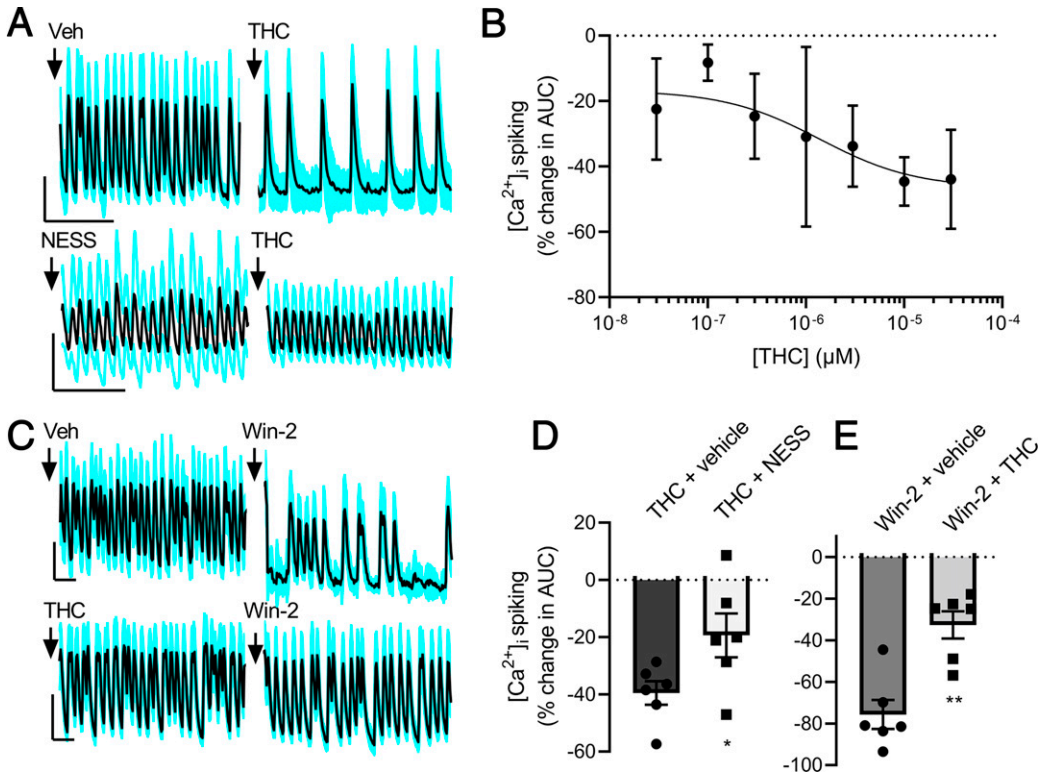

Fig. 4. Δ^9-THC acts as a partial agonist to inhibit synaptic transmission in hiPSC-derived neuronal cultures. (A) Representative traces show mean (solid line) $[Ca^{2+}]_i$ ($\Delta F/F_0$) of a single field of hiPSC-derived neuronal cells (S.D. denoted by blue shading) in 0.1 mM Mg^{2+} buffer before and after the addition of 1 μM Δ^9-THC in the absence (upper) or presence of 100 nM NESS 0327 (lower). Scale bars: horizontal, 30 seconds; vertical, 1.0 $\Delta F/F_0$. (B) Concentration-response curve for Δ^9-THC was fit with a logistic equation of the form percentage of change in AUC = $A_1 + [(A_2\text{-}A_1)/(1 + 10^{((\log x_0\text{-}x)p)})]$, where x_0 = EC_{50}, x = log[Δ^9-THC], A_1 = percentage of change in the absence of drug, A_2 = percentage of change at a maximally effective drug concentration, and p = slope factor. The following values were calculated using a nonlinear, least-squares curve-fitting program: $A_1 = -17 \pm 11\%$; $A_2 = -47 \pm 14\%$; $EC_{50} = 1.4 \pm 1.9$ μM; $p = -0.9 \pm 1.2$; n = 4–7 wells per concentration. (C) Representative traces show mean (solid line) $[Ca^{2+}]_i$ ($\Delta F/F_0$) of a single field of hiPSC-derived neuronal cells (S.D. denoted by blue shading) in 0.1 mM Mg^{2+} buffer before and after the addition of 1 μM Win-2 in the presence of vehicle (0.01% ethanol, top) or 1 μM Δ^9-THC (bottom). Scale bars: horizontal, 30 seconds; vertical, 1.0 $\Delta F/F_0$. (D) Bar graph shows change in $[Ca^{2+}]_i$ spiking relative to baseline (AUC) after addition of 1 μM Δ^9-THC in wells treated with vehicle or 100 nM NESS 0327. Data are presented as mean ± S.D. Unpaired Student's t test, $t_{(10)} = 2.3$, $^*P < 0.05$, n = 6 wells per condition. (E) Bar graph shows change in $[Ca^{2+}]_i$ spiking relative to baseline (AUC) after addition of 1 μM Win-2 in wells treated with vehicle or Δ^9-THC. Data are presented as mean ± S.D. Unpaired Student's t test, $t_{(5.5)} = 18.8$, $^{**}P < 0.0001$, n = 6 wells per condition. Veh, vehicle.

activity in rat hippocampal cultures (Wu and Thayer, 2020). Overall, these pharmacological studies indicate that hiPSC-derived neuronal cultures respond to both a synthetic cannabinoid and an eCB.

Δ^9-THC Acts as a Partial Agonist on CB_1R in hiPSC-Derived Neurons. Δ^9-THC, the principal psychoactive ingredient in marijuana, is a cannabinoid commonly used both medicinally and recreationally, which makes it important to test in this model system. Furthermore, Δ^9-THC acts as a partial agonist on both rodent and human $CB_{1/2}$Rs (Govaerts et al., 2004; Roloff and Thayer, 2009). Δ^9-THC inhibited 0.1 mM $[Mg^{2+}]_o$-evoked $[Ca^{2+}]_i$ spiking in a manner consistent with action as a partial agonist (Fig. 4). The IC_{50} of Δ^9-THC–mediated inhibition of $[Ca^{2+}]_i$ spiking was 1.4 ± 1.9 μM, a potency lower than that observed for Win-2 and comparable to that observed for 2-AG. A maximally effective concentration of Δ^9-THC elicited only 47 ± 14% inhibition (Fig. 4B), consistent with its partial agonist properties, and in contrast to the full agonists Win-2 and 2-AG (Fig. 3). The inhibition of $[Ca^{2+}]_i$ spiking evoked by 1 μM Δ^9-THC was significantly reduced in the presence of the CB_1R antagonist NESS 0327 (Fig. 4, A and D).

Because partial agonists occupy all the receptors at a maximally effective concentration, they can inhibit the activity of more efficacious agonists by competing for receptor binding sites. Indeed, 1 μM Δ^9-THC antagonized the activity of 1 μM Win-2 when added to the cultures 15 minutes before Win-2 (Fig. 4, C and E), confirming that Δ^9-THC acts as a partial CB_1R agonist in hiPSC-derived neuronal cultures.

hiPSC-Derived Neuronal Cultures Produce 2-AG via Diacylglycerol Lipase. We next investigated whether hiPSC-derived neuronal cultures produce eCBs in addition to responding to exogenously applied CBs. To detect eCB production, we used a G-protein-coupled receptor activation–based eCB ($GRAB_{eCB2.0}$) sensor (Dong et al., 2022). The sensor consists of a modified CB_1R fused to circularly permutated GFP such that it fluoresces upon ligand binding. We infected the hiPSC-derived neuronal cultures with an AAV vector that expressed $GRAB_{eCB2.0}$ under control of the neuron-specific human synapsin promoter ($AAV_{PHP.eB}$-hSyn-$GRAB_{eCB2.0}$). Six days after infection, the cultures expressed functional $GRAB_{eCB2.0}$ sensor, as evidenced by a large increase in fluorescence upon the addition of Win-2 (Fig. 5). The increase in $GRAB_{eCB\ 2.0}$ fluorescence evoked by 1 μM Win-2 was completely reversed by 100 nM NESS 0327 (n = 4).

Metabotropic suppression of excitation (MSE) is a form of synaptic modulation mediated by eCBs produced following

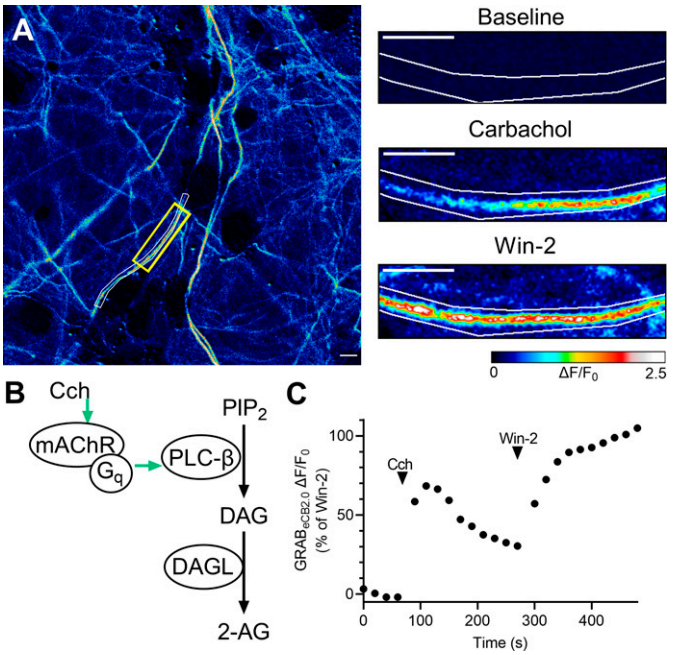

Fig. 5. eCB GRAB sensor imaging in hiPSC-derived neuronal cultures. (A) Left: $GRAB_{eCB2.0}$ fluorescence ($\Delta F/F_0$) in cells treated with 300 nM Win-2. Scale bar, 10 μm. Right: enlarged images of the boxed region at baseline (top) and after the addition of 1 μM carbachol (middle) and 300 nM Win-2 (bottom). Scale bar, 10 μm. (B) Schematic showing the mechanism of carbachol-triggered 2-AG synthesis. (C) Time course of $GRAB_{eCB2.0}$ fluorescence ($\Delta F/F_0$) for the ROI highlighted in (A) expressed as a percentage of the response in saturating Win-2 (mean of final 40 seconds of recording). Arrowheads mark the addition of 1 μM carbachol (Cch) and 300 nM Win-2. DAGL, diacylglycerol lipase; mAChR, muscarinic acetylcholine receptor; PIP_2, phosphatidylinositol bisphosphate; PLC-β, phospholipase C-β.

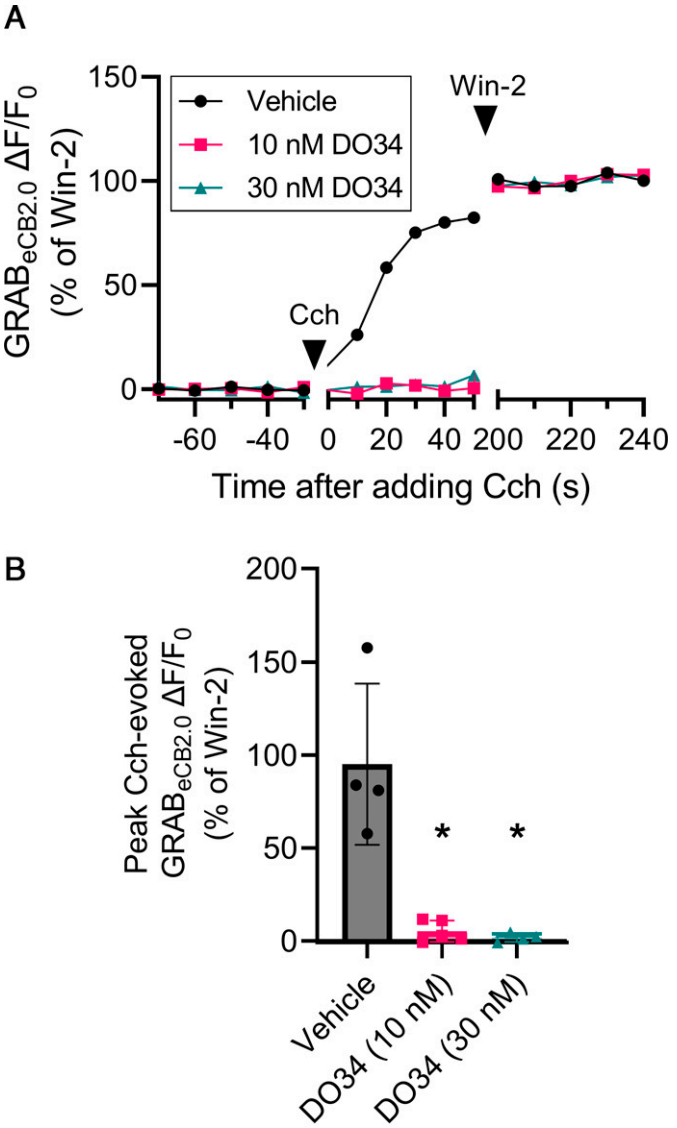

Fig. 6. hiPSC-derived neuronal cultures synthesize eCBs via DAG lipase. (A) Time courses showing mean $GRAB_{eCB2.0}$ fluorescence ($\Delta F/F_0$, expressed as a percentage of the Win-2 response) from representative wells pretreated for 1 hour with vehicle (0.1% DMSO) or 10 or 30 nM DO34. Arrowheads mark the addition of 1 μM carbachol (Cch) and 300 nM Win-2. n = 4 ROIs per well. (B) Bar graph summarizes peak carbachol-evoked $GRAB_{eCB2.0}$ fluorescence ($\Delta F/F_0$, expressed as a percentage of the Win-2 response) in wells pretreated for 1 hour with vehicle (0.1% DMSO), 10 nM DO34, or 30 nM DO34. Data are presented as mean ± S.D. *$P < 0.05$ relative to vehicle. Brown-Forsythe ANOVA test with Dunnet's T3 multiple comparisons test, $F_{(2.0,\ 3.1)} = 17.45$, $P = 0.045$ for 10 nM DO34 and 0.040 for 30 nM DO34 versus vehicle. n = 4 to 5 wells; each well is the average of 4 ROIs.

activation of G_q-coupled receptors that increase phospholipase C activity, leading to increased production of DAG from membrane phospholipids. Hydrolysis of DAG by DAG lipase increases levels of the eCB 2-AG, which subsequently activates presynaptic CB_1 receptors (Maejima et al., 2001a; Straiker and Mackie, 2007). MSE can be triggered by multiple G_q-coupled receptors, including muscarinic M1 receptors, which can be activated by the agonist carbachol (Martin et al., 2015). When carbachol (1 μM) was added to hiPSC-derived neuronal cultures expressing the $GRAB_{eCB2.0}$ sensor, fluorescence increased over 30–60 seconds to peak at 95 ± 43% of the maximum response to Win-2 (Fig. 5C; Fig. 6A). This indicates that the cultures are producing eCBs, likely 2-AG. To determine if carbachol was stimulating the production of 2-AG, we blocked DAG lipase activity with the potent inhibitor DO34. Preincubation with 10 or 30 nM DO34 for 60 minutes abolished the GRAB sensor response to carbachol (Fig. 6, A and B). This both confirms that the $GRAB_{eCB2.0}$ sensor is measuring eCB levels and indicates that 2-AG is the main eCB produced by carbachol stimulation of hiPSC-derived neuronal cultures.

hiPSC-Derived Cultures Metabolize 2-AG via Monoacylglycerol Lipase. After signaling, 2-AG is degraded by metabolic enzymes such as MAG lipase, which make up the final piece of a basic eCB system. Treating $GRAB_{eCB2.0}$-expressing hiPSC-derived neuronal cultures with 1 μM carbachol for 1 minute, followed by drug washout, produced a transient increase in fluorescence that returned to basal levels over approximately 5 minutes (Fig. 7A). This decay was not due to photobleaching of the $GRAB_{eCB2.0}$ sensor, because the signal induced by 1 μM Win-2 remained constant throughout the same imaging protocol (data not shown). To determine the role of MAG lipase in this recovery process, cultures were pretreated with vehicle (0.1% DMSO) or the irreversible MAG lipase inhibitor JZL184 for 1 hour before recording (Fig. 7A). When cultures were pretreated with JZL 184, the decay of the carbachol-induced $GRAB_{eCB2.0}$ signal was significantly slower (significant effect of time × treatment, 2-way repeated measures ANOVA, $F_{(29,\ 290)} = 3.064$, $P < 0.0001$). To compare recovery kinetics across multiple

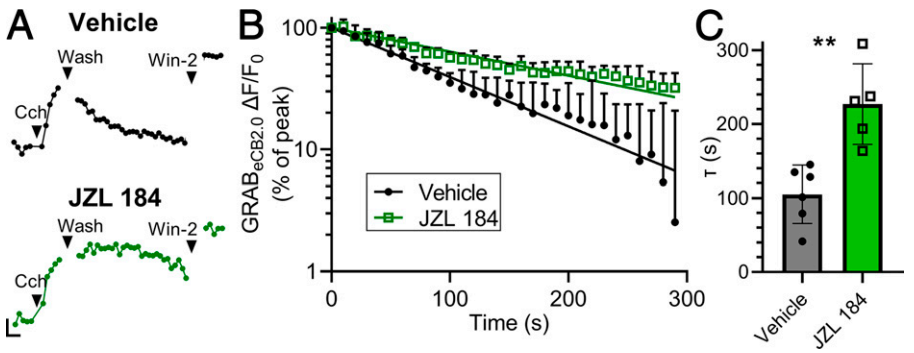

Fig. 7. hiPSC-derived neuronal cultures metabolize 2-AG via MAG lipase. (A) Traces showing average $GRAB_{eCB2.0}$ fluorescence from representative wells pretreated with vehicle or 1 μM JZL 184. Arrowheads show addition of 1 μM carbachol (Cch), washout of carbachol (wash), and addition of 300 nM Win-2. Each trace is the average of 4 ROIs from a single well. Scale bars: horizontal, 30 seconds; vertical, 20% of saturating Win-2 response ($\Delta F/F_0$). (B) Time course showing the decay of carbachol-evoked $GRAB_{eCB2.0}$ fluorescence after washout of carbachol ($\Delta F/F_0$, expressed as a percentage of the peak fluorescence on a log scale) in cells pretreated for 1 hour with vehicle (0.1% DMSO, filled circles) or 1 μM JZL 184 (open squares). One JZL 184 well decayed too slowly to calculate a time constant and is not included. $n = 6$ wells for vehicle and 5 wells for JZL 184. Data are presented as mean ± S.D. Curves were fit with a linear regression. (C) Bar graph shows time constants for $GRAB_{eCB2.0}$ fluorescence decay calculated from the individual recordings averaged in (B). Individual curves were fit with an exponential decay function constrained to a y-intercept of 100 and an asymptote approaching 0. Data are presented as mean ± S.D. $^{**}P < 0.01$. Unpaired Student's t test, $t_{(9)} = 4.5$, $n = 6$ wells for vehicle and 5 wells for JZL 184.

recordings, the recovery phase of each recording was normalized to peak and then averaged. The decay process was well fit by an exponential equation as shown by the linear regression fit to the data on a semilog plot (Fig. 7B). As shown in Fig. 7C, the time constant for recovery increased significantly from τ = 112 ± 28 seconds in vehicle-treated cultures to τ = 227 ± 55 seconds in cultures treated with JZL184 (excluding one JZL 184 recording in which the decay was too slow to calculate a time constant; Student's t test, $t_{(9)} = 4.5$, $P < 0.01$). This indicates that MAG lipase is degrading 2-AG produced by stimulating hiPSC-derived neuronal cultures with carbachol. Taken together, these results show that hiPSC-derived neuronal cultures contain a complete and functional eCB system.

Activation of Muscarinic Receptors in hiPSC-Derived Cultures Can Produce 2-AG Independent of $[Ca^{2+}]_i$. The enzymes responsible for 2-AG production, phospholipase C and DAG lipase (Fig. 5B), are stimulated by increases in $[Ca^{2+}]_i$ (Hashimotodani et al., 2005; Hashimotodani et al., 2008). Here, we examined the Ca^{2+} sensitivity of 2-AG production in hiPSC-derived neuronal cultures following activation of muscarinic receptors. Carbachol stimulates phospholipase C to hydrolyze phosphatidylinositol 4,5-bisphosphate (PIP_2) to inositol trisphosphate (IP_3) and DAG. IP_3 releases Ca^{2+} from endoplasmic reticulum (ER) stores. Thus, it was not surprising that neither the carbachol-evoked increase in $[Ca^{2+}]_i$ nor the evoked increase in 2-AG required extracellular Ca^{2+} (Fig. 8).

However, in cells pretreated for 30 minutes in nominally Ca^{2+}-free buffer with 1 μM thapsigargin, an agent that depletes ER Ca^{2+} stores by inhibiting the sarcoplasmic/endoplasmic reticulum Ca^{2+} ATPase, the carbachol-induced increase in $[Ca^{2+}]_i$ was completely blocked, whereas the evoked production of 2-AG was not affected (Fig. 8). Thus, Ca^{2+} mobilized from the ER does not appear to be required for 2-AG synthesis by this route, suggesting that a maximally effective concentration of carbachol triggers eCB production in a Ca^{2+}-independent manner in hiPSC-derived neuronal cultures.

CB_1R Desensitization Is Less Pronounced with a Metabolic Inhibitor than a Receptor Agonist in hiPSC-Derived Neuronal Cultures. Although Δ^9-THC and other CB_1R agonists show promise for treating a number of conditions, they carry the risk of tolerance and/or psychoactive side effects (Gorelick et al., 2013; Issa et al., 2014). One potential solution to avoid these adverse effects is to slow eCB metabolism instead, thus enhancing the endogenous spatial and temporal patterns of 2-AG signaling rather than activating all CB_1Rs for a prolonged period. We therefore tested whether the cannabinoid receptor agonist Win-2 and the MAG lipase inhibitor JZL 184 desensitized CB_1R-mediated presynaptic inhibition in hiPSC-derived neuronal cultures.

We used the 0.1 mM $[Mg^{2+}]_o$–evoked $[Ca^{2+}]_i$ spiking assay to test Win-2–mediated inhibition after treating the culture with vehicle, 1 μM Win-2, or 1 μM JZL184 for varying times (Fig. 9A), followed by a wash protocol described in *Methods*. A short (15-minute) treatment was used to validate the wash protocol. This brief treatment with vehicle, Win-2, or JZL 184 did not significantly affect the subsequent Win-2 test response. Thus, the wash protocol was sufficient to prevent any acute effects on CB_1R signaling resulting from carryover of the drug pretreatment.

The Win-2 test response was significantly attenuated in cultures pretreated with Win-2 for 1, 3, or 7 days before testing as opposed to those pretreated with vehicle (Fig. 9B). This indicates that Win-2 desensitizes the CB_1R in hiPSC-derived neurons. Exposing cultures to JZL 184, on the other hand, caused less pronounced desensitization of the Win-2 response. JZL 184 is an irreversible inhibitor of MAG lipase, so its duration of action is a function of the stability of JZL 184 as well as the turnover of MAG lipase protein. In control experiments, we found that the effects of JZL 184 were not significantly different when added once every 3 days with regular media changes or refreshed daily ($t_{(10)} = 0.4$, P = 0.70). Thus, for these experiments, fresh drug was only added at regular media changes. A 1-day exposure to JZL184 significantly attenuated the test response but did not completely block the CB_1R-mediated response, and even after 7 days, the desensitization was incomplete. This suggests that MAG lipase inhibition may be an effective strategy for avoiding tolerance when targeting the eCB system therapeutically.

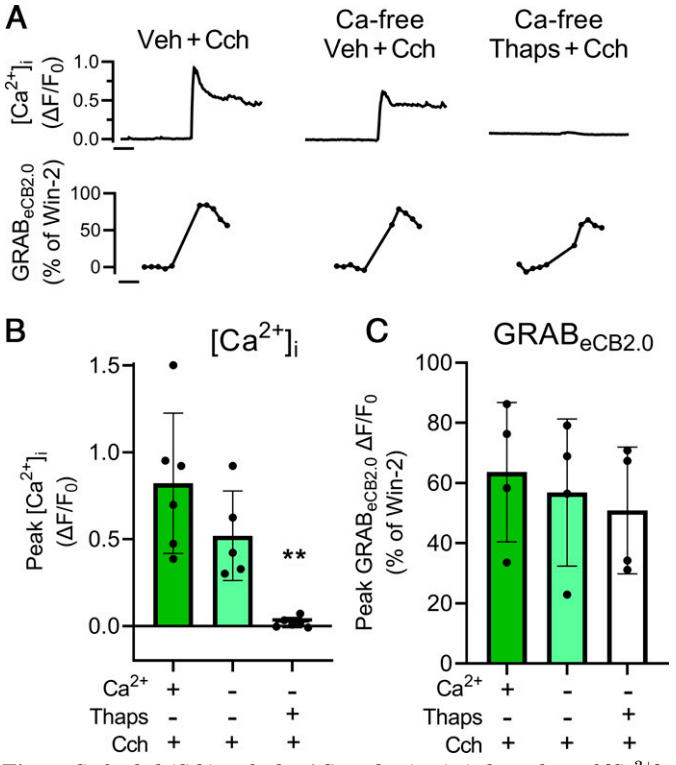

Fig. 8. Carbachol (Cch)-evoked 2-AG production is independent of $[Ca^{2+}]_i$. (A) Top: representative carbachol-evoked $[Ca^{2+}]_i$ traces from wells pretreated for 30 minutes with vehicle (0.1% DMSO) or 1 μM thapsigargin in the absence or presence of Ca^{2+} as indicated. Horizontal bar, 30 seconds. Bottom: representative traces showing $GRAB_{eCB2.0}$ fluorescence in wells pretreated as indicated. Horizontal bar, 30 seconds. (B) Bar graph summarizes peak increases in $[Ca^{2+}]_i$ evoked by 1 μM carbachol in the absence or presence of 1 μM thapsigargin. Recordings were performed in the absence (nominally Ca^{2+} free) or presence of 1.3 mM extracellular Ca^{2+} as indicated. $n = 6$ wells per condition. Data are presented as mean ± S.D. Brown-Forsythe ANOVA ($F_{(2, 8.4)} = 12.9$, $P = 0.0028$) with Dunnett's T3 multiple comparisons test $^{**}P < 0.01$, relative to vehicle + Ca^{2+} + carbachol. (C) Peak carbachol-evoked $GRAB_{eCB2.0}$ fluorescence in cells treated as indicated. $n = 4$ wells per condition; each well value is the average of 4 ROIs. Data are presented as mean ± S.D. Brown-Forsythe ANOVA $F_{(2, 8.9)} = 0.3$, $P = 0.75$. Thaps, thapsigargin; Veh, vehicle.

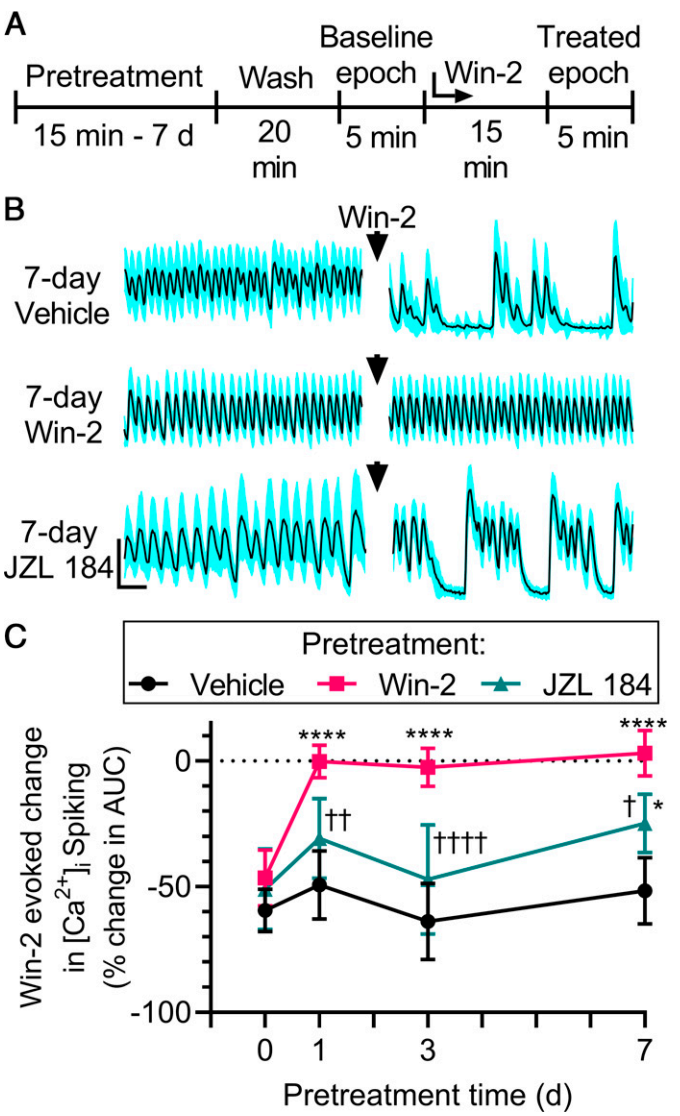

Fig. 9. Comparison of Win-2 to JZL184–induced desensitization of CB_1R-mediated inhibition of synaptic activity. (A) Timeline of pretreatment and imaging for desensitization experiments. (B) Representative traces show mean (solid line) $[Ca^{2+}]_i$ ($\Delta F/F_0$) of a single field of hiPSC-derived neuronal cells (S.D. denoted by blue shading) in 0.1 mM Mg^{2+} buffer before and after the addition of 1 μM Win-2 (arrowheads) in cells pretreated for 7 days with either vehicle (0.1% DMSO, top), 1 μM Win-2 (middle), or 1 μM JZL 184 (bottom). Scale bars: horizontal, 30 seconds; vertical, 1.0 $\Delta F/F_0$. (C) Plot shows inhibition of $[Ca^{2+}]_i$ spiking activity produced by 1 μM Win-2 in cells pretreated for the indicated times with vehicle (0.1% DMSO, black circles), 1 μM Win-2 (red squares), or 1 μM JZL 184 (green triangles). Data are presented as mean ± S.D. $n = 6$ wells per condition. $^{*}P < 0.05$ and $^{****}P < 0.0001$ relative to vehicle; †$P < 0.05$; ††$P < 001$; ††††$P < 0.0001$ relative to Win-2. Two-way repeated measures ANOVA with Tukey's multiple comparisons test. Pretreatment time $F_{(3, 59)} = 16.1$, $P < 0.0001$; pretreatment drug $F_{(2, 59)} = 67.2$, $P < 0.0001$, interaction $F_{(6, 59)} = 4.3$, $P = 0.0012$.

hiPSC-Derived Neuronal Lines from Multiple Sources Are Sensitive to CB_1R Agonists. The results presented thus far were generated from multiple platings of cells differentiated from a single iPSC line obtained from Stemonix, Inc. In Fig. 10, we show recordings from cultures obtained from additional commercial sources. In cells obtained from BrainXell, we observed asynchronous spontaneous $[Ca^{2+}]_i$ spiking activity that was not increased or synchronized by bathing the cells in 0.1 mM $Mg^{2+}{}_o$ (Fig. 10A). However, in those cells that exhibited spontaneous $[Ca^{2+}]_i$ spiking, 1 μM Win-2 inhibited the synaptic activity in a manner partially reversed by the CB_1R antagonist Ness 0327 (100 nM) (Fig. 10C). hiPSC-derived neuronal cultures produced from cells obtained from Applied StemCell exhibited synchronized $[Ca^{2+}]_i$ spiking activity in 0.1 mM $Mg^{2+}{}_o$ that was markedly inhibited by 1 μM Win-2 (Fig. 10, B and C). The effects of Win-2 were significantly reversed by Ness 0327 (100 nM). Thus, each of the three hiPSC-derived neuronal cultures exhibited synaptic activity that was inhibited by activation of CB_1Rs, suggesting that the results presented can be generalized, at least qualitatively, to multiple hiPSC-derived neuronal lines.

Discussion

Despite recent interest in the role of the ECS in neurologic disorders, there are few options for studying pathophysiological changes in the ECS or evaluating drugs that act on the ECS in

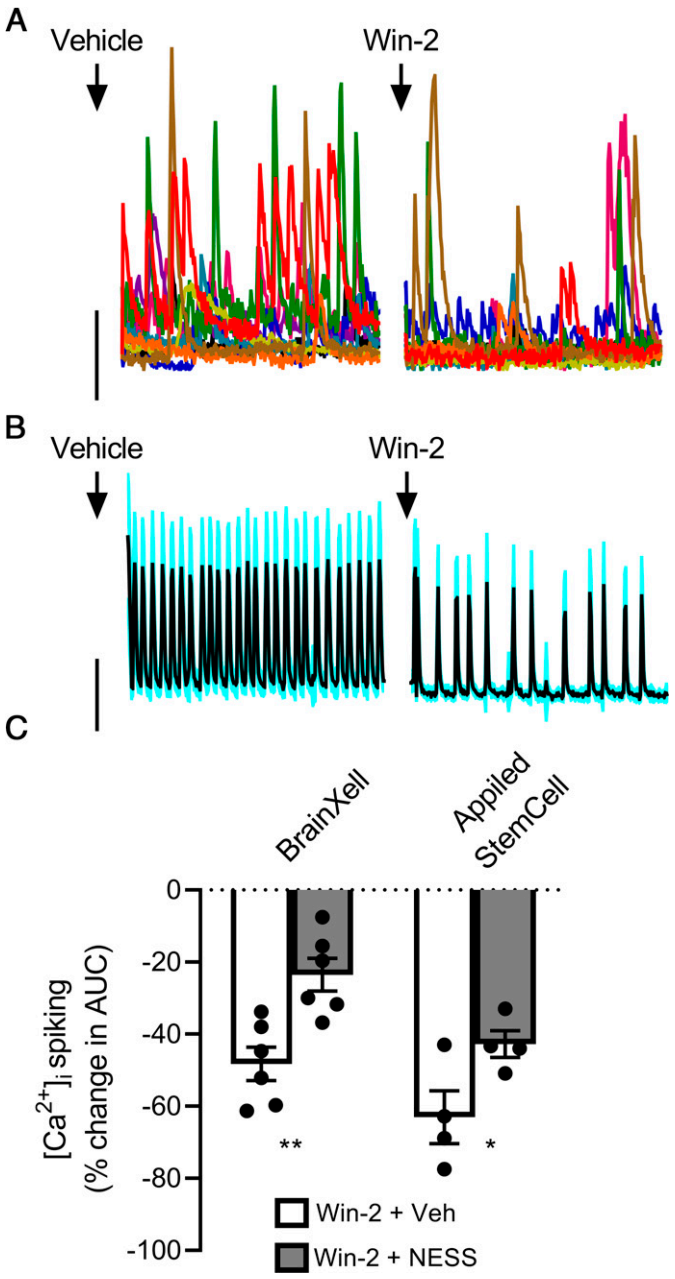

Fig. 10. CB_1R activation inhibits $[Ca^{2+}]_i$ spiking in hiPSC-derived neuronal cultures from multiple sources. (A) Individual $[Ca^{2+}]_i$ traces representing $\Delta F/F_0$ for spontaneously active ROIs in a cell culture produced from cells obtained from BrainXell. Recording was performed in 0.1 mM Mg^{2+} buffer, and cells were treated with 1 μM Win-2 at the time indicated by the arrow. Scale bar: horizontal, 30 seconds; vertical, 1.0 $\Delta F/F_0$. (B) Representative traces show mean (solid line) $[Ca^{2+}]_i$ ($\Delta F/F_0$) and S.D. (denoted by blue shading) from a single field of hiPSC-derived neuronal cells (obtained from Applied StemCell) in 0.1 mM Mg^{2+} buffer treated with 1 μM Win-2 at the time indicated by the arrow. Scale bars: horizontal, 30 seconds; vertical, 1.0 $\Delta F/F_0$. (C) Bar graph summarizes change in $[Ca^{2+}]_i$ spiking induced by 1 μM Win-2 in wells treated with vehicle (0.1% ethanol, open bars) or 100 nM NESS 0327 (filled bars) from cells obtained from BrainXell or Applied StemCell as indicated. Data are presented as mean ± S.D. $^*P < 0.05$; $^{**}P < 0.01$, unpaired Student's t test. For BrainXell hiPSCs, $t_{(10)} = 3.8$, $P = 0.003$, 6 wells per condition. For Applied StemCell hiPSCs, $t_{(6)} = 2.3$, $P = 0.049$, 4 wells per condition. Veh, vehicle.

human neurons. In this study, we show that hiPSC-derived neurons contain a functional ECS, providing a readily available human in vitro model for studying ECS neurophysiology and for drug discovery. hiPSC-derived neurons were amenable to useful functional assays, including Ca^{2+} imaging and a genetically encoded fluorescent cannabinoid sensor. Using these assays in combination with pharmacological tools, we demonstrate that the ECS is fully functional in hiPSC-derived neuronal cultures.

Although many studies to date involving cannabinoids and hiPSCs have examined the role of the $CB_{1/2}Rs$ in stem cell maintenance, differentiation, and synaptogenesis (Stanslowsky et al., 2017; Miranda et al., 2020; Shum et al., 2020), only a few have looked at the ECS in fully differentiated neurons. For example, Guennewig et al. (2018) examined Δ^9-THC–induced gene expression changes in hiPSC-derived neurons, finding that genes affected by Δ^9-THC exposure overlap partially with those that are altered in neuropsychiatric conditions, including schizophrenia. Because these cells responded to Δ^9-THC, it suggests that they express functional receptors, although the signal transduction pathways were not characterized in this study. Our study showed for the first time that CB_1R agonists inhibit synaptic transmission between hiPSC-derived neurons. Taken together, these studies suggest that it may be possible to relate cannabinoid-induced changes in synaptic function to altered gene expression in human neurons. We also determined the concentration dependence of CB_1R agonists. They were less potent in hiPSC-derived neuronal cultures than in primary rat hippocampal cultures previously studied by our laboratory (Figs. 3 and 4) (Shen et al., 1996; Wu and Thayer, 2020). This may result from species differences in receptor sensitivity, in agreement with previous studies showing that Win-2 acted on human CB_1Rs with lower affinity than on rat receptors (McPartland et al., 2007). There could also be effects of culture type (iPSC-derived versus primary), brain region (cortex-like versus hippocampus), or sex (one male human donor versus a mix of male and female rats).

We demonstrate for the first time that hiPSC-derived neuronal cultures express a fully functional ECS that modulates synaptic transmission via CB1Rs and synthesizes and metabolizes 2-AG. Our study, which focuses on the pharmacological characterization and evaluation of ECS function, compliments another recent study in an hiPSC-derived cortical spheroid model, which demonstrated expression of the ECS components that we assessed functionally. Using immunofluorescence and quantitative reverse-transcription polymerase chain reaction, Papariello et al. (2021) found CB_1R, DAG lipase, and MAG lipase were expressed in cortical spheroids. Together with this study, our $[Ca^{2+}]_i$ imaging and eCB sensor data provide solid evidence that the ECS is both present and functional in hiPSC-derived neurons. Importantly, the cortical spheroids used by Papariello et al. (2021) used dual-SMAD inhibition (Chambers et al., 2009) for neural induction, whereas our two-dimensional cultures used an embryonic body-based induction protocol (Marchetto et al., 2010). This, along with our observation that hiPSC-derived neurons from multiple commercial sources are sensitive to CB_1R agonists, suggests that ECS expression and function are present in a variety of different hiPSC-derived neurons and are not peculiar to one cell line, method, or source.

In addition to responding to exogenously applied cannabinoids, hiPSC-derived neuronal cultures also produced eCBs in response to carbachol. 2-AG is likely the main carbachol-evoked eCB in this system because its synthesis and degradation were blocked by inhibitors of DAG lipase and MAG lipase, respectively. This does not, however, rule out the possibility

that the hiPSC-derived cultures can produce other eCBs, perhaps with different stimuli. Furthermore, the carbachol-evoked $GRAB_{eCB2.0}$ response continued to recover in the presence of JZL 184 despite being significantly slowed, suggesting that other degradative enzymes such as α/β-hydrolase domain-containing 6 (Zhang et al., 2021) might be present in hiPSC-derived neuronal cultures.

There are multiple ways to evoke eCB synthesis, with different levels of Ca^{2+} dependence. In general, depolarization-induced suppression of excitation, in which voltage-gated Ca^{2+} channels are activated, requires an influx of extracellular Ca^{2+} (Ohno-Shosaku et al., 2001), whereas MSE, in which Gq-coupled receptors activate PLC, is either Ca^{2+} independent (Maejima et al., 2001b) or partially dependent on Ca^{2+} release from intracellular ER stores (Robbe et al., 2002). Our data support the hypothesis that MSE is calcium independent in hiPSC-derived neurons, based on the fact that nominally calcium-free buffer combined with thapsigargin abolished the carbachol-evoked $[Ca^{2+}]_i$ response but not carbachol-evoked eCB production. Because we did not add a Ca^{2+} chelator to our Ca^{2+}-free media, we cannot entirely rule out the possibility that trace amounts of Ca^{2+} are required for eCB synthesis; however, the carbachol-evoked increase in $[Ca^{2+}]_i$ was undetectable by the Calcium 6 dye. Submaximal stimulation of the metabotropic receptor and voltage-gated Ca^{2+} influx pathways display synergistic activation of 2-AG synthesis (Hashimotodani et al., 2005). However, our experiments were not designed to detect enhancement of submaximal DAG lipase activation. Our study does illustrate the utility of hiPSC-derived neuronal cultures for the mechanistic study of the ECS.

It is important to study the complete eCB system to understand how drugs that act selectively on a single element of the ECS affect the other components indirectly. The desensitization experiments performed in this study illustrate this point. CB_1Rs are downregulated or desensitized with prolonged exposure to ligand (Kouznetsova et al., 2002), making tolerance an obstacle to drug development. Indeed, heavy cannabis use can lead to Δ^9-THC tolerance and dependence in humans (Colizzi and Bhattacharyya, 2018) and rodents (González et al., 2005), and the CB_1R is downregulated in postmortem human brain tissue from frequent cannabis users relative to nonusers (Villares, 2007). Previous studies have investigated JZL 184–induced CB_1R desensitization in rodents, with mixed results. Schlosburg et al. (2010) found that a 6-day treatment with JZL 184 led to tolerance in mice as measured by antinociceptive effects, and CB_1R binding sites were reduced in several brain regions, including cortex. Conversely, Feliszek et al. (2016) saw only mild receptor desensitization in the hippocampus after 14-day exposure to the same dose; they also noted that the amount of desensitization was dose and age dependent. Our results in adult human iPSC–derived neuronal cultures support the hypothesis that JZL 184 causes slower and/or less pronounced desensitization than a CB_1R agonist. Future studies using multiple concentrations and longer pretreatment times could further clarify the best way to administer inhibitors of 2-AG metabolism for the most benefit with the least tolerance. The desensitization experiment also highlights the stability of the hiPSC cultures. Although our treatment protocol was 7 days in duration, we have used cultures as old as 15 weeks, suggesting that extended drug exposures are feasible in hiPSC-derived neuronal cultures that are not possible in rodent primary cultures.

hiPSC-derived neuronal cultures show promise for studying human neurological disorders because they can be derived from patient tissue samples (Okano and Morimoto, 2022). Understanding how the ECS is affected in inherited human disease may identify novel insights into pathophysiological changes. In a study of fetal brain development, comparing cells derived from children with autism to those derived from typically developing controls revealed that expression of both diacylglycerol lipase and MAGL was increased in autism, highlighting the usefulness of hiPSC-derived neurons that express the ECS for studying neurodevelopmental disorders (Papariello et al., 2021).

Here, we focused on the effects of cannabinoids on a glutamatergic network; however, the CB_1R is expressed at very high levels in GABAergic interneurons (Marsicano and Lutz, 2006) and at lower levels in astrocytes (Navarrete and Araque, 2008). These other cell types contribute to more complex activity patterns, which are outside the scope of this study. In addition, MAGL inhibitors do not only increase eCB signaling—they also reduce inflammation by blocking the production of arachidonic acid from 2-AG (Long et al., 2009). Microglia play a large role in neuroinflammation but are not present in the cultures used in this study. Although microglia arise from a yolk sac lineage and cannot easily be produced from the same differentiation protocol as neurons and astrocytes, they can be derived separately and cocultured with other cell types of interest [reviewed in Hasselmann and Blurton-Jones (2020)]. Development of coculture models may help to elucidate the full effects of MAGL inhibitors in the future.

In conclusion, human iPSC–derived neuronal cultures recapitulate a diverse suite of eCB functions, providing a minimally invasive and potentially high-throughput human platform for eCB research and drug discovery.

Acknowledgments

We thank Ezequiel Maron and the University of Minnesota Viral Vector Cloning Core for preparing adeno-associated viral vectors used in this study.

Authorship Contributions

Participated in research design: Asher, Thayer.
Conducted experiments: Asher, McMullan.
Contributed new reagents or analytic tools: Dong, Li.
Performed data analysis: Asher, McMullan.
Wrote or contributed to the writing of the manuscript: Asher, Thayer, McMullan.

References

Bara A, Ferland JN, Rompala G, Szutorisz H, and Hurd YL (2021) Cannabis and synaptic reprogramming of the developing brain. *Nat Rev Neurosci* **22**:423–438.
Bobrov, M. Y., Bezuglov, V. V., Khaspekov, L. G., Illarioshkin, S. N., Novosadova, E. V., and Grivennikov, I. A. (2017). Expression of Type I Cannabinoid Receptors at Different Stages of Neuronal Differentiation of Human Fibroblasts. *Bulletin of Experimental Biology and Medicine*, **163**(2), 272–275. https://doi.org/10.1007/s10517-017-3782-2
Chambers SM, Fasano CA, Papapetrou EP, Tomishima M, Sadelain M, and Studer L (2009) Highly efficient neural conversion of human ES and iPS cells by dual inhibition of SMAD signaling. *Nat Biotechnol* **27**:275–280.
Chan, K. Y., Jang, M. J., Yoo, B. B., Greenbaum, A., Ravi, N., Wu, W. L., Sánchez-Guardado, L., Lois, C., Mazmanian, S. K., Deverman, B. E., and Gradinaru, V. (2017). Engineered AAVs for efficient noninvasive gene delivery to the central and peripheral nervous systems. *Nature Neuroscience*, **20**(8), 1172–1179.

Chen, S., Sun, S., Moonen, D., Lee, C., Lee, A. Y. F., Schaffer, D. V., and He, L. (2019). CRISPR-READI: Efficient Generation of Knockin Mice by CRISPR RNP Electroporation and AAV Donor Infection. *Cell Reports*, **27**(13), 3780–3789.e4. https://doi.org/10.1016/j.celrep.2019.05.103

Colizzi M and Bhattacharyya S (2018) Cannabis use and the development of tolerance: a systematic review of human evidence. *Neurosci Biobehav Rev* **93**:1–25.

deRoon-Cassini TA, Stollenwerk TM, Beatka M, and Hillard CJ (2020) Meet Your Stress Management Professionals: The Endocannabinoids. *Trends Mol Med* **26**:953–968.

Di Marzo, V. New approaches and challenges to targeting the endocannabinoid system. *Nat Rev Drug Discov* **17**, 623–639 (2018). https://doi.org/10.1038/nrd.2018.115

Dong A, He K, Dudok B, Farrell JS, Guan W, Liput DJ, Puhl HL, Cai R, Wang H, Duan J, et al. (2022) A fluorescent sensor for spatiotemporally resolved imaging of endocannabinoid dynamics in vivo. *Nat Biotechnol* **40**:787–798.

van Egmond N, Straub VM, and van der Stelt M (2021) Targeting Endocannabinoid Signaling: FAAH and MAG Lipase Inhibitors. *Annu Rev Pharmacol Toxicol* **61**:441–463.

Feliszek M, Bindila L, Lutz B, Zimmer A, Bilkei-Gorzo A, and Schlicker E (2016) Lack of hippocampal CB1 receptor desensitization by Δ(9)-tetrahydrocannabinol in aged mice and by low doses of JZL 184. *Naunyn Schmiedebergs Arch Pharmacol* **389**:603–612.

Fowler CJ (2021) The endocannabinoid system - current implications for drug development. *J Intern Med* **290**:2–26.

Garcia JM and Shamliyan TA (2018) Cannabinoids in Patients with Nausea and Vomiting Associated with Malignancy and Its Treatments. *Am J Med* **131**:755–759.e2.

Glass M, Dragunow M, and Faull RL (1997) Cannabinoid receptors in the human brain: a detailed anatomical and quantitative autoradiographic study in the fetal, neonatal and adult human brain. *Neuroscience* **77**:299–318.

González S, Cebeira M, and Fernández-Ruiz J (2005) Cannabinoid tolerance and dependence: a review of studies in laboratory animals. *Pharmacol Biochem Behav* **81**:300–318.

Gorelick DA, Goodwin RS, Schwilke E, Schwope DM, Darwin WD, Kelly DL, McMahon RP, Liu F, Ortemann-Renon C, Bonnet D, et al. (2013) Tolerance to effects of high-dose oral δ9-tetrahydrocannabinol and plasma cannabinoid concentrations in male daily cannabis smokers. *J Anal Toxicol* **37**:11–16.

Govaerts SJ, Hermans E, and Lambert DM (2004) Comparison of cannabinoid ligands affinities and efficacies in murine tissues and in transfected cells expressing human recombinant cannabinoid receptors. *Eur J Pharm Sci* **23**:233–243.

Green MV, Pengo T, Raybuck JD, Naqvi T, McMullan HM, Hawkinson JE, Marron Fernandez de Velasco E, Muntean BS, Martemyanov KA, Satterfield R, et al. (2019) Automated Live-Cell Imaging of Synapses in Rat and Human Neuronal Cultures. *Front Cell Neurosci* **13**:467.

Guennewig B, Bitar M, Obiorah I, Hanks J, O'Brien EA, Kaczorowski DC, Hurd YL, Roussos P, Brennand KJ, and Barry G (2018) THC exposure of human iPSC neurons impacts genes associated with neuropsychiatric disorders. *Transl Psychiatry* **8**:89.

Gulyás-Kovács A, Dóczi J, Tarnawa I, Détári L, Banczerowski-Pelyhe I, and Világi I (2002) Comparison of spontaneous and evoked epileptiform activity in three in vitro epilepsy models. *Brain Res* **945**:174–180.

Hashimotodani, Y., Ohno-Shosaku, T., Maejima, T., Fukami, K., and Kano, M. (2008). Pharmacological evidence for the involvement of diacylglycerol lipase in depolarization-induced endocanabinoid release. *Neuropharmacology*, **54**(1), 58–67. https://doi.org/10.1016/j.neuropharm.2007.06.002

Hashimotodani Y, Ohno-Shosaku T, Tsubokawa H, Ogata H, Emoto K, Maejima T, Araishi K, Shin HS, and Kano M (2005) Phospholipase Cbeta serves as a coincidence detector through its Ca2+ dependency for triggering retrograde endocannabinoid signal. *Neuron* **45**:257–268.

Hasselmann J and Blurton-Jones M (2020) Human iPSC-derived microglia: A growing toolset to study the brain's innate immune cells. *Glia* **68**:721–739.

Issa MA, Narang S, Jamison RN, Michna E, Edwards RR, Penetar DM, and Wasan AD (2014) The subjective psychoactive effects of oral dronabinol studied in a randomized, controlled crossover clinical trial for pain. *Clin J Pain* **30**:472–478.

Kouznetsova M, Kelley B, Shen M, and Thayer SA (2002) Desensitization of cannabinoid-mediated presynaptic inhibition of neurotransmission between rat hippocampal neurons in culture. *Mol Pharmacol* **61**:477–485.

Leo LM and Abood ME (2021) CB1 Cannabinoid Receptor Signaling and Biased Signaling. *Molecules* **26**:5413.

Long JZ, Nomura DK, and Cravatt BF (2009) Characterization of monoacylglycerol lipase inhibition reveals differences in central and peripheral endocannabinoid metabolism. *Chem Biol* **16**:744–753.

Lowe H, Toyang N, Steele B, Bryant J, and Ngwa W (2021) The Endocannabinoid System: A Potential Target for the Treatment of Various Diseases. *Int J Mol Sci* **22**:9472.

Lu HC and Mackie K (2021) Review of the Endocannabinoid System. *Biol Psychiatry Cogn Neurosci Neuroimaging* **6**:607–615.

Maejima T, Hashimoto K, Yoshida T, Aiba A, and Kano M (2001a) Presynaptic inhibition caused by retrograde signal from metabotropic glutamate to cannabinoid receptors. *Neuron* **31**:463–475.

Maejima T, Ohno-Shosaku T, and Kano M (2001b) Endogenous cannabinoid as a retrograde messenger from depolarized postsynaptic neurons to presynaptic terminals. *Neurosci Res* **40**:205–210.

Marchetto MC, Carromeu C, Acab A, Yu D, Yeo GW, Mu Y, Chen G, Gage FH, and Muotri AR (2010) A model for neural development and treatment of Rett syndrome using human induced pluripotent stem cells. *Cell* **143**:527–539.

Marsicano G and Lutz B (2006) Neuromodulatory functions of the endocannabinoid system. *J Endocrinol Invest* **29**(3, Suppl)27–46.

Martin HG, Bernabeu A, Lassalle O, Bouille C, Beurrier C, Pelissier-Alicot AL, and Manzoni OJ (2015) Endocannabinoids Mediate Muscarinic Acetylcholine Receptor-Dependent Long-Term Depression in the Adult Medial Prefrontal Cortex. *Front Cell Neurosci* **9**:457.

Matsuda LA, Lolait SJ, Brownstein MJ, Young AC, and Bonner TI (1990) Structure of a cannabinoid receptor and functional expression of the cloned cDNA. *Nature* **346**:561–564.

McLeod Jr JR, Shen M, Kim DJ, and Thayer SA (1998) Neurotoxicity mediated by aberrant patterns of synaptic activity between rat hippocampal neurons in culture. *J Neurophysiol* **80**:2688–2698.

McPartland JM, Glass M, and Pertwee RG (2007) Meta-analysis of cannabinoid ligand binding affinity and receptor distribution: interspecies differences. *Br J Pharmacol* **152**:583–593.

Miranda CC, Barata T, Vaz SH, Ferreira C, Quintas A, and Bekman EP (2020) hiPSC-Based Model of Prenatal Exposure to Cannabinoids: Effect on Neuronal Differentiation. *Front Mol Neurosci* **13**:119.

Navarrete M and Araque A (2008) Endocannabinoids mediate neuron-astrocyte communication. *Neuron* **57**:883–893.

Ohno-Shosaku T, Maejima T, and Kano M (2001) Endogenous cannabinoids mediate retrograde signals from depolarized postsynaptic neurons to presynaptic terminals. *Neuron* **29**:729–738.

Okano H and Morimoto S (2022) iPSC-based disease modeling and drug discovery in cardinal neurodegenerative disorders. *Cell Stem Cell* **29**:189–208.

Papariello A, Taylor D, Soderstrom K, and Litwa K (2021) CB_1 antagonism increases excitatory synaptogenesis in a cortical spheroid model of fetal brain development. *Sci Rep* **11**:9356.

Robbe D, Kopf M, Remaury A, Bockaert J, and Manzoni OJ (2002) Endogenous cannabinoids mediate long-term synaptic depression in the nucleus accumbens. *Proc Natl Acad Sci USA* **99**:8384–8388.

Roloff AM and Thayer SA (2009) Modulation of excitatory synaptic transmission by Delta 9-tetrahydrocannabinol switches from agonist to antagonist depending on firing rate. *Mol Pharmacol* **75**:892–900.

Rosenberg EC, Patra PH, and Whalley BJ (2017) Therapeutic effects of cannabinoids in animal models of seizures, epilepsy, epileptogenesis, and epilepsy-related neuroprotection. *Epilepsy Behav* **70**:319–327.

Ruiu S, Pinna GA, Marchese G, Mussinu JM, Saba P, Tambaro S, Casti P, Vargiu R, and Pani L (2003) Synthesis and characterization of NESS 0327: a novel putative antagonist of the CB1 cannabinoid receptor. *J Pharmacol Exp Ther* **306**:363–370.

Schlosburg JE, Blankman JL, Long JZ, Nomura DK, Pan B, Kinsey SG, Nguyen PT, Ramesh D, Booker L, Burston JJ, et al. (2010) Chronic monoacylglycerol lipase blockade causes functional antagonism of the endocannabinoid system. *Nat Neurosci* **13**:1113–1119.

Shen M, Piser TM, Seybold VS, and Thayer SA (1996) Cannabinoid receptor agonists inhibit glutamatergic synaptic transmission in rat hippocampal cultures. *J Neurosci* **16**:4322–4334.

Shum C, Dutan L, Annuario E, Warre-Cornish K, Taylor SE, Taylor RD, Andreae LC, Buckley NJ, Price J, Bhattacharyya S, et al. (2020) Δ^9-tetrahydrocannabinol and 2-AG decreases neurite outgrowth and differentially affects ERK1/2 and Akt signaling in hiPSC-derived cortical neurons. *Mol Cell Neurosci* **103**:103463.

Stanslowsky N, Jahn K, Venneri A, Naujock M, Haase A, Martin U, Frieling H, and Wegner F (2017) Functional effects of cannabinoids during dopaminergic specification of human neural precursors derived from induced pluripotent stem cells. *Addict Biol* **22**:1329–1342.

Straiker A and Mackie K (2005) Depolarization-induced suppression of excitation in murine autaptic hippocampal neurones. *J Physiol* **569**:501–517.

Straiker A and Mackie K (2007) Metabotropic suppression of excitation in murine autaptic hippocampal neurons. *J Physiol* **578**:773–785.

Takahashi, K., Tanabe, K., Ohnuki, M., Narita, M., Ichisaka, T., Tomoda, K., and Yamanaka, S. (2007). Induction of Pluripotent Stem Cells from Adult Human Fibroblasts by Defined Factors. *Cell*, **131**(5), 861–872. https://doi.org/10.1016/j.cell.2007.11.019

Tukker, A. M., Wijnolts, F. M. J., de Groot, A., and Westerink, R. H. S. (2020). Applicability of hiPSC-derived neuronal co-cultures and rodent primary cortical cultures for in vitro seizure liability assessment. *Toxicological Sciences*. https://doi.org/10.1093/toxsci/kfaa136

Villares J (2007) Chronic use of marijuana decreases cannabinoid receptor binding and mRNA expression in the human brain. *Neuroscience* **145**:323–334.

Wilkerson, J. L., Bilbrey, J. A., Felix, J. S., Makriyannis, A., and McMahon, L. R. (2021). Untapped endocannabinoid pharmacological targets: Pipe dream or pipeline? *Pharmacology Biochemistry and Behavior*, **206**(September 2020), 173192. https://doi.org/10.1016/j.pbb.2021.173192

Wu MM and Thayer SA (2020) HIV Tat Protein Selectively Impairs CB_1 Receptor-Mediated Presynaptic Inhibition at Excitatory But Not Inhibitory Synapses. *eNeuro* **7**:ENEURO.0119-20.2020.

Zhang H, Li X, Liao D, Luo P, and Jiang X (2021) Alpha/Beta-Hydrolase Domain-Containing 6: Signaling and Function in the Central Nervous System. *Front Pharmacol* **12**:784202.

Address correspondence to: Stanley A. Thayer, Department of Pharmacology; University of Minnesota Medical School, 6-120 Jackson Hall, 321 Church Street SE, Minneapolis, MN 55455. E-mail: sathayer@umn.edu